Collision Avoidance for Non-Cooperative Multi-Swarm Coverage Control with Measurement Uncertainty

Karolina Schmidt

A Thesis
in
The Department
of
Electrical and Computer Engineering

Presented in Partial Fulfillment of the Requirements
For the Degree of Master of Applied Science in Electrical and Computer Engineering
Concordia University
Montréal, Québec, Canada

August 2025

Concordia University

School of Graduate Studies

This is to certify that the thesis prepared

By: Karolina Schmidt

Entitled: Collision Avoidance for Non-Cooperative Multi-Swarm Coverage Control with Measurement Uncertainty

and submitted in partial fulfillment of the requirements for the degree of

Master of Applied Science in Electrical and Computer Engineering

complies with the regulations of this university and meets the accepted standards with respect to originality and quality.

Signed by the final Examining Committee:

________________________________ Chair

Dr. A. Hamou-Lhadj

________________________________ External Examiner

Dr. W. Xie

________________________________ Examiner

Dr. S. Hashtrudi Zad

________________________________ Supervisor

Dr. L. Rodrigues

Approved by ________________________________

Dr. A. Hamou-Lhadj, Chair
Department of Electrical and Computer Engineering

__________ 2025 __________________________

Dr. M. Debbabi, Dean
Faculty of Engineering and Computer Science

Abstract

Collision Avoidance for Non-Cooperative Multi-Swarm Coverage Control with Measurement Uncertainty

Karolina Schmidt

The main focus of this thesis is to provide strategies for collision-free motion in multi-swarm coverage control. Motivated by the diverse use of agent-based systems for various tasks, the scenario of multiple non-cooperating swarms independently covering a common area is presented. Using Voronoi tessellation in coverage control, collision-free motion of agents within the same swarm has been proven before. However, in the case of multiple swarms following their own objectives, these guarantees do not hold. To address this issue, the Optimal Reciprocal Collision Avoidance (ORCA) method used for safe navigation in multi-agent scenarios is applied to multi-swarm coverage control. Assuming knowledge regarding the positions of all agents, the proposed methodology is formally analyzed for planar motion and validated through Monte Carlo simulations. Subsequently, the collision-avoidance algorithm is investigated in environments where bounded disturbance measurement uncertainties are present. To account for these disturbances, an extension of ORCA is proposed. Formal guarantees are presented for motion without collisions between agents. This is done under the assumption that the input needed to counteract the disturbance can always be achieved. The theoretical results are applied to coverage control of multiple non-cooperating swarms and validated through MATLAB simulations.

Acknowledgments

I am extremely pleased with the successful completion of my master's studies, which would not have been possible without my family. My sincere gratitude to my father Karsten, my mother Susanne, and my brother Bastian. Your support, encouragement, and inspiration are the greatest gifts I could ever wish for. Thank you for your pleasant visits and for always warmly welcoming me at your home.

I also express my deepest appreciation to my supervisor, Dr. Luis Rodrigues, for his exceptional guidance and invaluable support. Thank you for patiently sharing your immense expertise and for your knowledgeable advice. I would also like to gratefully acknowledge CRIAQ, CAE, and RWDI for the opportunity to work on their fascinating and innovative projects and for generously funding my research.

Special thanks to Zachary, Camilo, Lucas, Mohammad, and Steven for being the best colleagues I could have asked for. It has been a great pleasure to work with you, and I am looking forward to continuing to do so. Thank you, Steven, for being a great fellow adventurer and travel companion, but most importantly, an amazing friend.

Last but not least, I very much appreciate the great company of my roommates Cristina, Ethan, and Yelena. Many thanks also to my teammates and coaches on my two soccer teams, Concordia Women's Reserve and CS Montréal-Centre, for offering a pleasant atmosphere to help me stay physically fit and mentally balanced.

Contents

List of Figures

List of Algorithms

Chapter 1

Introduction

1.1 Motivation

Due to the various tasks that swarms of agents are intended to execute, there is a need for multiple non-cooperating swarms to independently provide maximum coverage to a common area. Applications include wildfire management, where search and rescue operations must be performed simultaneously with fire monitoring and other tasks. Moreover, additional examples are planetary exploration where swarms belonging to different countries compete to cover as much terrain as possible, and mobile network coverage for remote areas or places with temporarily increased network load provided by drones from different companies.

An important consideration to guarantee safe navigation in all of these scenarios, as well as in other applications, is the avoidance of collisions between agents. This includes the necessity to compensate for wind when Unmanned Aerial Vehicles (UAVs) are deployed, or currents when Autonomous Underwater Vehicles (AUVs) are involved. The following subsections examine the need for coverage control within multiple non-cooperating swarms.

1.1.1 Wildfire Management

In recent years, wildfires have raised concerns within Canada and throughout the world. In 2023, Canadian forests suffered record-breaking destruction caused by wildfires. The *Internal Displacement Monitoring Centre* [5] reports that in that year 43 percent of global wildfires occurred in Canada. According to the *Government of Canada* [6] more than 6000 fires affected an area of 15 million hectares, which is more than 4 percent of the country's overall forest area ranging over 367 million hectares [7]. A map of wildfire perimeters across Canada in 2023 is shown in figure 1.1.

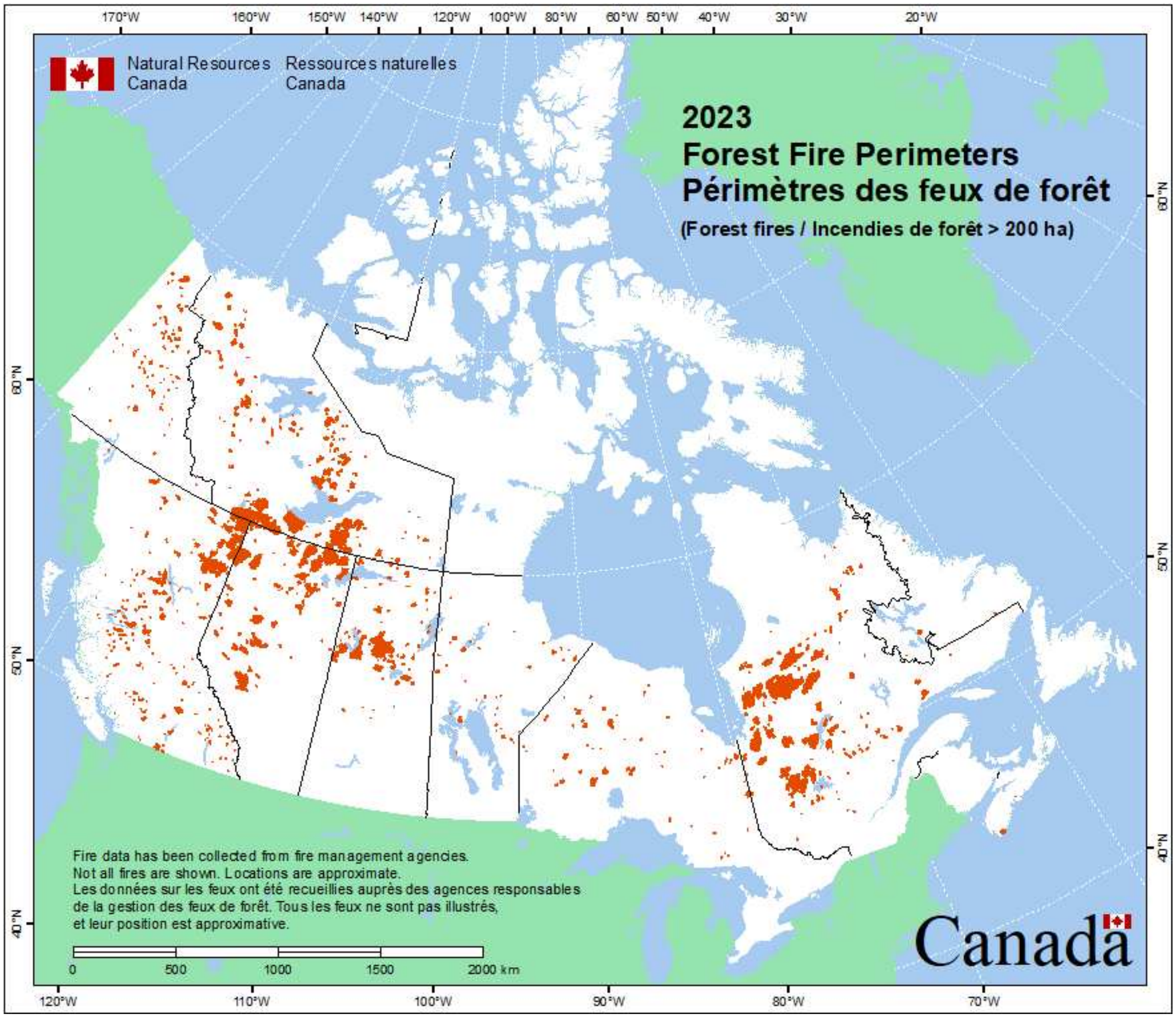
170°W
160°W
150°W
140°W
120°W
100°W
80°W
60°W
50°W
40°W
30°W
20°W
Natural Resources Canada
Ressources naturelles Canada
2023
Forest Fire Perimeters
Périmètres des feux de forêt
(Forest fires / Incendies de forêt > 200 ha)
60°N
50°N
40°N
Fire data has been collected from fire management agencies.
Not all fires are shown. Locations are approximate.
Les données sur les feux ont été recueillies auprès des agences responsables
de la gestion des feux de forêt. Tous les feux ne sont pas illustrés,
et leur position est approximative.
0
500
1000
1500
2000 km
Canada
120°W
110°W
100°W
90°W
80°W
70°W

Figure 1.1: Map of wildfire perimeters across Canada in 2023 [1]

Not only do wildfires destroy nature and properties, but they also release large amounts of greenhouse gases such as carbon dioxide and hazardous pollutants, making them contributors to climate change and threats to public health [8]. In addition to the hazards posed to populations, firefighting teams risk their lives to extinguish fires and save their fellows. To ensure security for individuals and communities while monitoring affected areas, a strong need for reliable means of assistance arises.

In that sense, the use of Unmanned Aerial Vehicles (UAVs) has gained importance in recent years. Applications include search and rescue missions to trace missing people, as well as fire mapping and monitoring. In addition, firefighting systems based on swarms of UAVs are conceivable. They promise higher deployment speeds than manned aircraft, reduced limitations due to factors such as visibility and water refueling, and elimination of missions that threaten pilot lives [9].

In these contexts, it is common for UAVs to work in collaborative units rather than individually to pursue a mutual goal. A prevalent example for operations in wildfire management is the provision of maximum coverage over an area of interest with a swarm of multiple UAVs. As a result of the various tasks that swarms are intended to execute, a need for multiple swarms operating within the same area arises. Collision avoidance between agents from the same swarm as well as different swarms must then be guaranteed. Moreover, since wildfires commonly occur in remote areas where UAVs are exposed to winds of high intensities, drifts due to wind and measurement uncertainty must be taken into account.

1.1.2 Planetary Exploration

Space-related competition between countries has been going on since the mid-20th century, when the *Union of Soviet Socialist Republics* launched the first artificial satellite [10]. Besides the advancement of satellite technologies and missions focusing on human spaceflight, the exploration of our solar system and beyond plays a crucial role. One component is planetary exploration. Notable missions are conducted on Mars. These include missions performed by the US-American *National Aeronautics and Space Administration (NASA)*'s active rovers

Curiosity and *Perserverance* and their precursors, as well as *NASA*'s Mars helicopter *Ingenuity* [11, 12]. A photo of *Ingenuity* taken by *Perserverance* on August 2, 2023 is shown in figure 1.2. Moreover, after their deployment of Mars rover *Zhurong* the *People's Republic of China* plans to continue the exploration of the red planet in their *Tianwen-3* mission in 2028 [13]. A rover called *Rosalind Franklin* is scheduled to launch in 2028 within the scope of the *European Space Agency*'s *ExoMars* program [14].

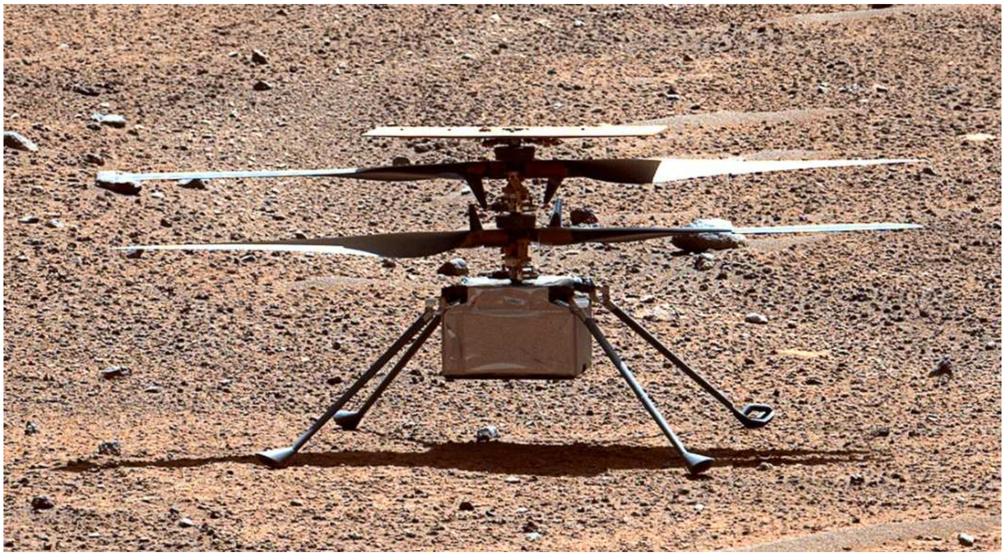

Figure 1.2: Photo of *Ingenuity* taken by *Perserverance* on August 2, 2023 [2]

Although the above planetary exploration missions are conducted by independent rovers rather than swarms of vehicles, multi-agent systems represent a promising solution for future operations. One potential solution is the concept of so-called *Marsbees* developed by researchers from the *United States of America* and *Japan* [15]. A *Marsbee* is a flapping-wing flyer the size of a bumblebee. In addition to the characteristic that a *Marsbee* can generate sufficient lift to hover in Mars' thin atmosphere, the deployment of multiple *Marsbees* as a swarm provides a resilient system and can increase the total area covered within a given time. Another proposal of a multi-agent system for planetary exploration is the use of two-wheeled robotic swarms [16].

It is apparent that when multiple swarms of agents operating on the ground or in the air and belonging to different countries explore a common area, collisions between agents must be avoided. Wind or other disturbances, along with measurement uncertainties that evidently appear in unexplored environments, can complicate this challenge.

1.1.3 Drone-based Mobile Networks

Drone-based Mobile Networks have gained attention in recent years. Especially in rural and remote areas that are difficult to reach, UAVs promise to be a competitive and cost-effective alternative to conventional stationary mobile network infrastructure consisting of cell towers. Similarly, UAVs can provide a simple and flexible solution for mobile coverage after disaster events such as earthquakes, floods, and wildfires. A crucial factor to increase the chances of survival of missing people is communication and connectivity between rescuers. UAVs can quickly establish a flexible network when stationary infrastructure is not available or destroyed [17]. In recent years, the company *Zhongxing Telecommunication Equipment Corporation (ZTE)* has developed and deployed airborne base stations in China to ensure communication during and after natural disasters [18].

In addition to that, UAVs can provide a simple and effective solution in scenarios where reinforced network capacity is temporarily needed, for example, during large-scale events. In February 2025, the first deployment of a UAV acting as a base station in Europe was performed during the cross-country ski race *Jizerská* in the Czech Republic [19].

Although to date most applications used individual agents rather than swarms of multiple UAVs, potential future enhancements include cooperation of multiple agents to jointly establish stronger networks and increase reliability. To allow maximum coverage of the mobile network, UAVs acting as airborne cell towers must be positioned accordingly. However, similarly to stationary networks, it is likely that multiple companies will compete to offer mobile network services within the same area. Therefore, it is crucial for UAVs belonging to different companies to not collide with each other. Disturbances such as wind cause additional difficulties. In particular, when UAVs are deployed after natural disasters that involve storms, winds can reach high intensities and are difficult to predict.

1.2 Literature Survey

1.2.1 Coverage Control

Coverage control has been a widely studied subject during the past two decades. The use of centroidal Voronoi partitions and proximity graphs for coverage control was first investigated by Cortés et al. in references [20, 21]. Using Lloyd's iterative algorithm [22] and gradient descent methods, a swarm of agents is coordinated to provide maximum coverage for an area. Furthermore, guarantees for the convergence of the algorithms are studied. Applications of centroidal Voronoi tessellations are discussed in [23].

Extensions and further advances are proposed, among others, in reference [24] where energy conservation and efficiency are considered by formulating an optimal control problem. Reference [25] addresses the same problem for discrete-time systems. Moreover, analytic expressions for the rate of change of the mass and the location of the center of mass of a Voronoi cell are introduced in reference [26].

More recent work on coverage control includes the presentation of approaches to avoid obstacles within the area to be covered. In reference [27], a controller based on control barrier functions is proposed to restrict the system to maintain a safe state. The authors of reference [28] present a method using an ant colony algorithm for agents to achieve coverage of an area while avoiding collisions with static obstacles.

A common feature of the above references is the consideration of one single swarm of agents working as a team towards a common goal. In reference [29], more than one swarm of vehicles is incorporated into a multi-agent scenario. However, the objective is multi-agent formation rather than coverage control. Coverage control using a group of Unmanned Ground Vehicles along with a swarm of UAVs was considered in reference [30]. The work focuses on collaboration between the two swarms that cover the given area as a unit. Moreover, reference [31] investigates the use of more than one swarm of vehicles to cover larger areas in less time. To achieve this, a leader-follower approach is adopted. Similarly to reference [30], different swarms jointly work towards a common goal. The division of a unit of robots into subgroups of similar size that work towards one common goal is studied in [32]. The work focuses on increasing the regional coverage speed and reducing the moving distances of the agents.

In practice, uncertainty is an important consideration in control systems of all types. For coverage control with a single swarm, reference [33] addresses bounded measurement errors in the positions of the agents. The focus is on the reduction of the effects of the bounded position measurement errors on the convergence to a configuration that entails optimal coverage of an area. Reference [34] proposes two variants of the Voronoi tessellation to account for position uncertainty while avoiding collisions with other agents that are part of the swarm. Reference [35] presents a leader-follower approach to avoid collisions with obstacles in coverage control scenarios. The work addresses actuator faults and time-varying uncertainties, but followers are restricted to stay within the sensing range of the leader, which limits the size of the area that can be covered. The authors of [35] extend their work in reference [36] using a controller based on control barrier functions. Specifically, the controller addresses the loss of controllability due to actuator faults and time-varying disturbances. All of the above consider one swarm only rather than multiple.

1.2.2 Collision Avoidance with Velocity Obstacles

The velocity obstacles (VO) technique was first introduced in reference [3]. It performs operations within the velocity space to select maneuvers that lead to avoidance of static and moving obstacles. Assuming obstacles with constant velocities and directions of motion, agents select their velocity outside a subset of the velocity space called the Velocity Obstacle containing all velocities that would result in collision at a future time.

An extension of VO was proposed in reference [37]. To make the method suitable for multi-agent systems, the authors assumed similar avoidance strategies of the obstacles and considered their reactive behavior. Further research on the extension and improvement of VO for multi-agent navigation includes the introduction of truncated collision cones in reference [38]. An optimization problem is formulated to ensure collision-free motion in multi-agent situations. Furthermore, the work includes considerations for computational efficiency through data and thread-level parallelism. The authors of [4] adopted the idea of Velocity Obstacles in the form of truncated cones and derived a method called Optimal Reciprocal Collision Avoidance (ORCA). ORCA achieves collision-free motion in multi-agent systems with independently operating agents by deriving half-spaces of permitted velocities so that a low-dimensional linear program can be solved to obtain local collision avoidance. A detailed overview of collision avoidance methods based on VO is given in [39]. Note that the above references do not consider the effects of disturbances and uncertainties.

Although in general VO methods are not concerned with uncertainties, modifications that account for deviations and noise have been presented over the years. Reference [40] extends the original VO method to account for stochastic uncertainties in the position and velocity of moving obstacles. The approach enlarges the collision cone computed by VO and combines it with an artificial potential field to include a buffer zone between an agent and an obstacle. Another approach based on the original VO method that accounts for uncertainties in the movement of obstacles due to sensor deviations is presented in reference [41]. The authors use a cost function to determine a collision-free velocity of an agent. Reference [42] presents a motion planning strategy that bounds the risk of collision in multi-agent systems. The collision avoidance strategy presented is based on VO and accounts for Gaussian noise in the system dynamics, model uncertainty, and uncertainty in the initial positions of the agents.

Independent of VO and its extensions, reference [43] presents a control strategy to avoid collisions between two agents. Bounded uncertainties in the positions of the agents due to sensing errors are addressed. Moreover, the effects of random wind on collision avoidance are analyzed in reference [44].

1.3 Contributions

The main contributions of the work presented in this thesis are the following:

1. In Chapter 3, the scenario of multiple non-cooperating swarms that independently cover a common area is introduced. In contrast to previous work, distinct swarms act as entirely independent units without explicitly exchanging information. An algorithm for collision-free motion in Voronoi-based coverage control is proposed based on ORCA. Although ORCA was introduced in reference [4], to the best of our knowledge, there are no theorems available in the open literature that prove collision avoidance. In contrast with the literature, Chapter 3 provides formal guarantees for collision-free motion when ORCA is used. Monte Carlo simulations validate the results.

2. Chapter 4 addresses the problem introduced in Chapter 3 in the presence of bounded measurement uncertainties. A methodology is presented that accounts for these perturbations. Formal guarantees for collision avoidance are given under the assumption that the input needed to counteract disturbances can always be achieved. An algorithm for coverage control with multiple non-cooperating swarms is then proposed. MATLAB simulations confirm the validity of the results.

1.4 Thesis Structure

The structure of this thesis is as follows. Chapter 2 introduces preliminary notions and definitions, including Delaunay graphs and Voronoi tessellation, coverage control and related work on energy efficiency, as well as the original VO method with its extension called ORCA. In Chapter 3, the scenario of multiple non-cooperating swarms in coverage control is presented, along with formal guarantees for collision avoidance using ORCA, and an algorithm that combines multi-swarm coverage control with ORCA to avoid collisions between agents. Examples and Monte Carlo simulations validate the results. Subsequently, Chapter

4 proposes a methodology for collision-free motion in multi-agent scenarios with bounded disturbance measurement uncertainties. After analyzing the influences of disturbances on the motion of an agent, an extended version of ORCA is presented and formalized that accounts for bounded measurement uncertainties. The proposed methodology is applied to multi-swarm coverage control in an algorithm. Simulations that validate the results are shown. Conclusions are drawn in Chapter 5.

Chapter 2

Mathematical Preliminaries

2.1 Introduction

This chapter summarizes underlying notions as well as definitions introduced in the related literature. After a brief description of Voronoi tessellation and Delaunay Graphs in section 2.2, some concepts of Voronoi-based coverage control are described in section 2.3 following [20, 21]. A comprehensive summary is given in [24]. The consideration of energy efficiency and conservation in coverage control as introduced in [24] is explained in section 2.4. Section 2.5 presents the original VO method as introduced in [3]. The version of VO that this work is based on, ORCA [4], is summarized in section 2.6.

2.2 Voronoi Tessellation and Delaunay Graphs

Consider n distinct points referred to as generators located within a convex area Q. Voronoi tessellation is obtained by partitioning Q into subsets. Each generator $p_i, i \in \{1, ..., n\}$ is associated with one subset called Voronoi cell $V_i(P), i \in \{1, ..., n\}$, where $P = \{p_1, ..., p_n\} \subset Q$. Voronoi cells take the shape of a convex polytope, where the Lebesgue measure of the boundaries between Voronoi cells is zero. In a two-dimensional scenario, the boundary between Voronoi cells corresponding to neighboring generators is defined by a straight line.

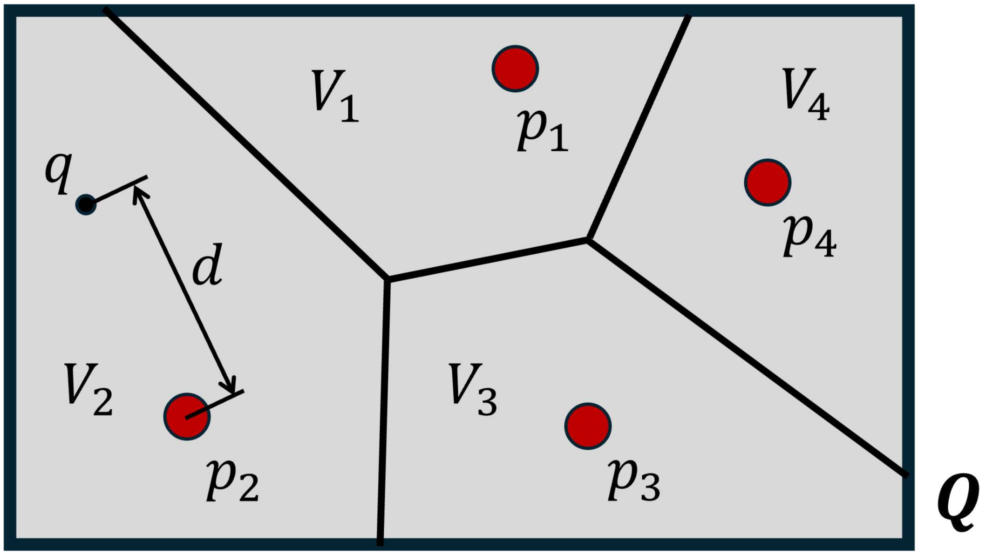

Figure 2.1: Voronoi tessellation of an area Q containing four generators

Each point on the line is equidistant from the locations of the two respective generators. The partition into Voronoi cells is performed so that the distance from any point $q \in Q$ to the generator of its Voronoi cell is less than or equal to the distance to any other generator p_j. Voronoi tessellation with the generators located at the center of mass of their Voronoi cells is called a centroidal Voronoi configuration. Figure 2.1 shows an example of a non-centroidal Voronoi diagram for an area containing four generators.

A Delaunay graph is a proximity graph related to Voronoi tessellation. It is obtained by connecting neighboring generators. The line connecting two neighboring generators is perpendicular to the shared boundary of their Voronoi cells. A visualization of a Delaunay graph is given in figure 2.2. The Delaunay graph is shown in solid black lines. Dashed gray lines represent the Voronoi tessellation.

2.3 Coverage Control

One field of application of Voronoi tessellation is multi-agent coverage control. Multi-agent coverage control deals with the problem of deploying a number n of collaborating agents so that maximum coverage of a given area Q is achieved. The positions of the agents are denoted

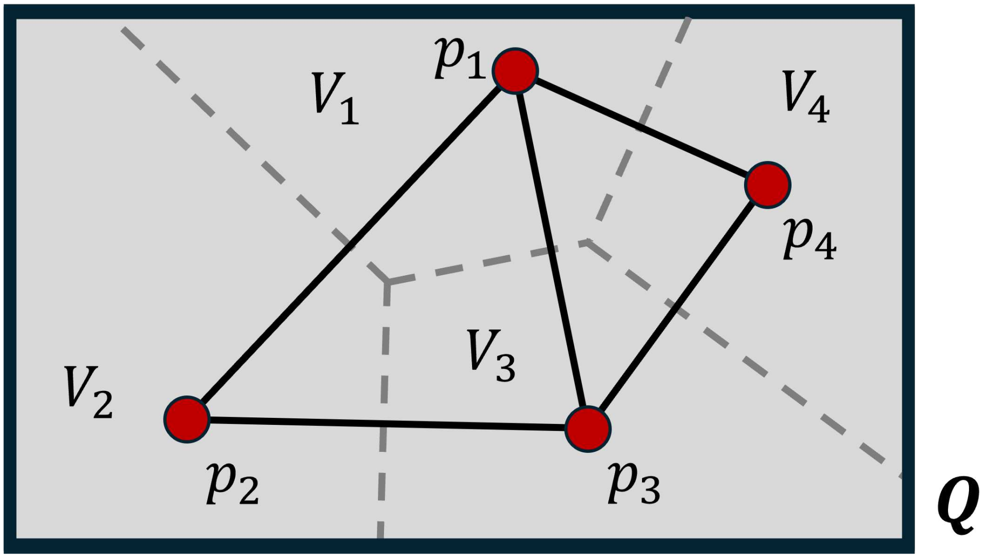

Figure 2.2: Delaunay triangulation (solid black lines) for an area Q with four generators. Voronoi tessellation is displayed in dashed gray lines.

by $X = \{x_1, ..., x_n\}$, where $x_i \in Q, i \in \{1, ..., n\}$. Then, to obtain a Voronoi tessellation of Q, each agent i acts as a generator for its respective Voronoi cell V_i. Each point $q \in Q$ is associated with its closest agent which provides coverage at q,

$$V_i(X) = \{q \in Q \mid \|q - x_i\| \leq \|q - x_j\| \, \forall x_j \in X\}. \tag{2.1}$$

Coverage at a point $q \in Q$ is inversely proportional to the square of the distance from q to the agent located closest to q, here indicated by $i(q)$. A distance function is described as $f(x_{i(q)}, q) = ||x_{i(q)} - q||^2$. High distance values correspond to a low level of coverage, whereas low values indicate high coverage.

Moreover, the priority of coverage at q is described by a density function $\phi(q)$. Therefore, a function that indicates the poorness of coverage over Q is [24],

$$V(x) = \int_Q ||x_{i(q)} - q||^2 \phi(q) dq, \tag{2.2}$$

where $x = [x_1, ..., x_n]^T$. To maximize overall coverage over Q, $V(x)$ is minimized. By rewriting (2.2) to consider all Voronoi cells V_i individually instead of Q as a whole and summing up the results, one obtains

$$V(x) = \sum_{i=1}^{n} \int_{V_i} ||x_{i(q)} - q||^2 \phi(q) dq. \tag{2.3}$$

The necessary condition for a local minimum of $V(x)$ is [24]

$$\begin{aligned} \frac{\partial V}{\partial x_j} &= 2 \int_{V_j} (x_j - q)^T \phi(q) dq \\ &= 2 \left(\int_{V_j} \phi(q) dq \right) \left(x_j - \frac{\int_{V_j} q\phi(q) dq}{\int_{V_j} \phi(q) dq} \right)^T \\ &= 0. \end{aligned} \tag{2.4}$$

Note that equation (2.4) contains a term for the mass M_{V_j} of Voronoi cell V_j,

$$M_{V_j} = \int_{V_j} \phi(q) dq, \tag{2.5}$$

and a term for its center of mass CM_{V_j},

$$CM_{V_j} = \frac{\int_{V_j} q\phi(q) dq}{\int_{V_j} \phi(q) dq} = \frac{\int_{V_j} q\phi(q) dq}{M_{V_j}}. \tag{2.6}$$

Equation (2.4) can therefore be rewritten as

$$\frac{\partial V}{\partial x_j} = 2M_{V_j}(x_j - CM_{V_j})^T = 0. \tag{2.7}$$

Clearly, this condition holds when $x_j = CM_{V_j}$, indicating that agent j is located at the center of mass of its Voronoi cell V_j. With the mass always being positive, the sufficient condition for a local minimum of V is satisfied,

$$\frac{\partial^2 V}{\partial x_j^2} = 2M_{V_j} > 0. \tag{2.8}$$

When each agent is located at the center of mass of its Voronoi cell, a centroidal Voronoi configuration is obtained.

To move each agent towards the center of mass of its Voronoi cell, a commonly used strategy is Lloyd's algorithm [22]. Iteratively, agents compute the center of mass of their Voronoi cells and select velocity vectors pointing in the respective direction. A first order dynamical model for the closed-loop dynamics of each agent is thus

$$\begin{aligned} \dot{x}_i &= u_i, \\ u_i &= k_i(CM_{V_i} - x_i), \end{aligned} \tag{2.9}$$

with u_i being the control input of agent i and where $k_i > 0$. Notice that agents slow down as they get closer to their target position. Using LaSalle's invariance principle, it can be concluded that the system converges to a centroidal Voronoi configuration [24].

2.4 Energy-Efficient Coverage Control

The authors of [24] formulate the coverage task as the following optimal control problem,

$$\begin{aligned} &\underset{u_i, i\in\{1,\ldots,n\}}{inf} \int_0^\infty \sum_{i=1}^n \left(s_i || \int_{V_i} (x_i - q)\phi(q)dq||^2 + r_i u_i^T u_i \right) d\tau \\ &s.t.\ \dot{x}_i = u_i. \end{aligned} \tag{2.10}$$

The coefficients $s_i \geq 0$ and $r_i > 0$ weigh the importance of coverage as measured by the coverage criterion

$$M_{V_i}||x_i - CM_{V_i}|| = || \int_{V_i} (x_i - q)\phi(q)dq||, \tag{2.11}$$

and energy used by each agent, respectively. The authors of reference [24] prove that the optimal solution to (2.10) that is spatially distributed over Delaunay graphs is

$$u_i = -\sqrt{s_i/r_i} \int_{V_i} (x_i - q)\phi(q)dq. \tag{2.12}$$

In this thesis, we will consider the following first order dynamical model for the dynamics of each agent,

$$\begin{aligned}\dot{x}_i &= u_i,\\ u_i &= k_i(CM_{V_i} - x_i),\end{aligned} \tag{2.13}$$

with

$$k_i = M_i\sqrt{s_i/r_i}. \tag{2.14}$$

In reference [24], using LaSalle's invariance principle, the authors prove that agents with dynamics as in (2.13) converge to a centroidal Voronoi configuration.

2.5 Velocity Obstacles

The original method of VO was first introduced in [3]. This section summarizes the concept. Consider a robot A and an obstacle B, both spherical. The respective positions, as well as the velocities v_A and v_B are assumed to be known. Denoting the radii as r_A and r_B, respectively, A is represented as a point mass $\hat{A}$, while $\hat{B}$ represents B enlarged by r_A. A collision cone $CC_{A,B}$ is then defined as [3]

$$CC_{A,B} = \left\{ v_{A,B} \,\middle|\, \lambda_{A,B} \cap \hat{B} \neq \emptyset \right\}, \tag{2.15}$$

where $v_{A,B} = v_A - v_B$ is the relative velocity of $\hat{A}$ with respect to $\hat{B}$, and $\lambda_{A,B}$ is the line of $v_{A,B}$ passing through $\hat{A}$. $CC_{A,B}$ is the set of relative velocities between $\hat{A}$ and $\hat{B}$ that result in a collision if both v_A and v_B are constant. It has its apex at $\hat{A}$ and is bounded by two lines λ_f and λ_r, which are tangent to $\hat{B}$ and pass through $\hat{A}$. Relative velocities outside $CC_{A,B}$ will not entail a collision. The geometry of $CC_{A,B}$ is visualized in figure 2.3a.

An equivalent condition is obtained by translating $CC_{A,B}$ by v_B to obtain the Velocity

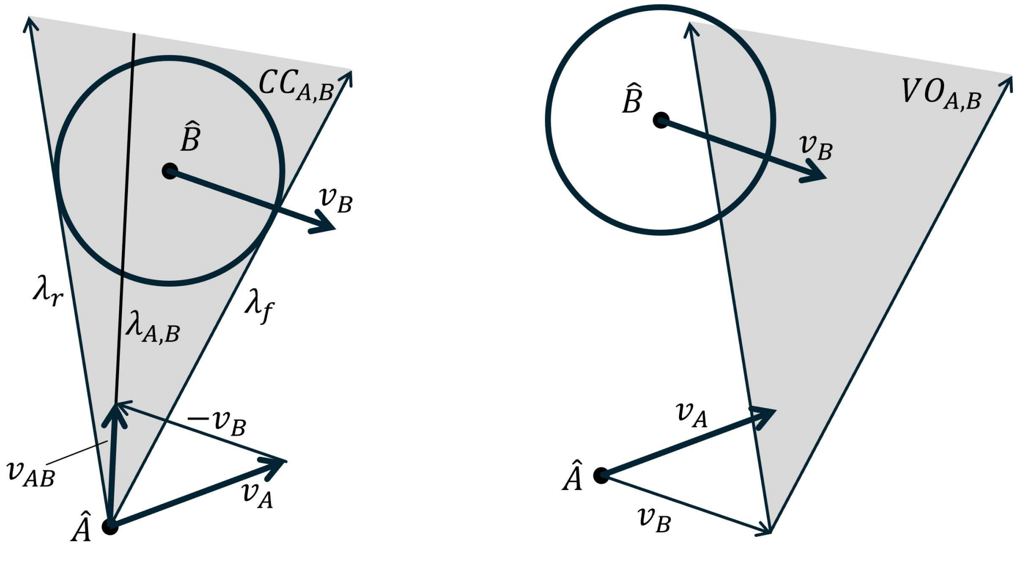

(a)

(b)

Figure 2.3: Visualization of (a) Collision Cone $CC_{A,B}$ and (b) Velocity Obstacle $VO_{A,B}$, adapted from [3]

Obstacle,

$$VO_{A,B} = CC_{A,B} + v_B = \{c + v_B \,|c \in CC_{A,B}\}\,. \tag{2.16}$$

In that case, to avoid collisions A must choose its velocity, so that

$$v_A \notin VO_{A,B}. \tag{2.17}$$

A visual representation of $VO_{A,B}$ is shown in figure 2.3b. To consider multiple obstacles, the union of the Velocity Obstacles with respect to each obstacle is computed,

$$VO = \cup_{i-1}^{m} VO_{A,B_i}, \tag{2.18}$$

with m being the total number of obstacles. To avoid collisions, A must then choose its new velocity outside VO,

$$v_A \notin VO. \tag{2.19}$$

2.6 Optimal Reciprocal Collision Avoidance

This section summarizes the work presented in reference [4]. Consider two spherical agents A and B with radii r_A and r_B and centered at positions x_A and x_B, respectively.

Definition 2.1. *A collision between two spherical agents A and B occurs when*

$$\|x_A - x_B\| \leq r_A + r_B. \tag{2.20}$$

Conversely, the agents do not collide when

$$\|x_A - x_B\| > r_A + r_B. \tag{2.21}$$

Using ORCA, agent A can compute the so-called Velocity Obstacle of A with respect to B for time horizon τ, denoted as $\mathcal{VO}^{\tau}_{AB}$, which is a truncated collision cone in the velocity space. It is proven in section 3.4 that assuming A and B keep their velocities constant for at least τ instants of time, the agents collide if and only if their relative velocity $v_A - v_B$ falls within $\mathcal{VO}^{\tau}_{AB}$. The Velocity Obstacle $\mathcal{VO}^{\tau}_{AB}$ is computed as [4]

$$\mathcal{VO}^{\tau}_{AB} = \{v \,|\, \exists t \in (0, \tau] : v \in D((x_B - x_A)/t, (r_A + r_B)/t)\}, \tag{2.22}$$

where

$$D(x, r) = \{q \,|\, \|q - x\| \leq r\}. \tag{2.23}$$

A visualization of $\mathcal{VO}^{\tau}_{AB}$ is shown in figure 2.4.

Let v_A^{pref} and v_B^{pref} be the desired velocities that A and B aim to follow, respectively, to meet other potential path planning objectives. To avoid a collision with B, A computes the shortest vector from

$$v_{AB}^{pref} = v_A^{pref} - v_B^{pref} \tag{2.24}$$

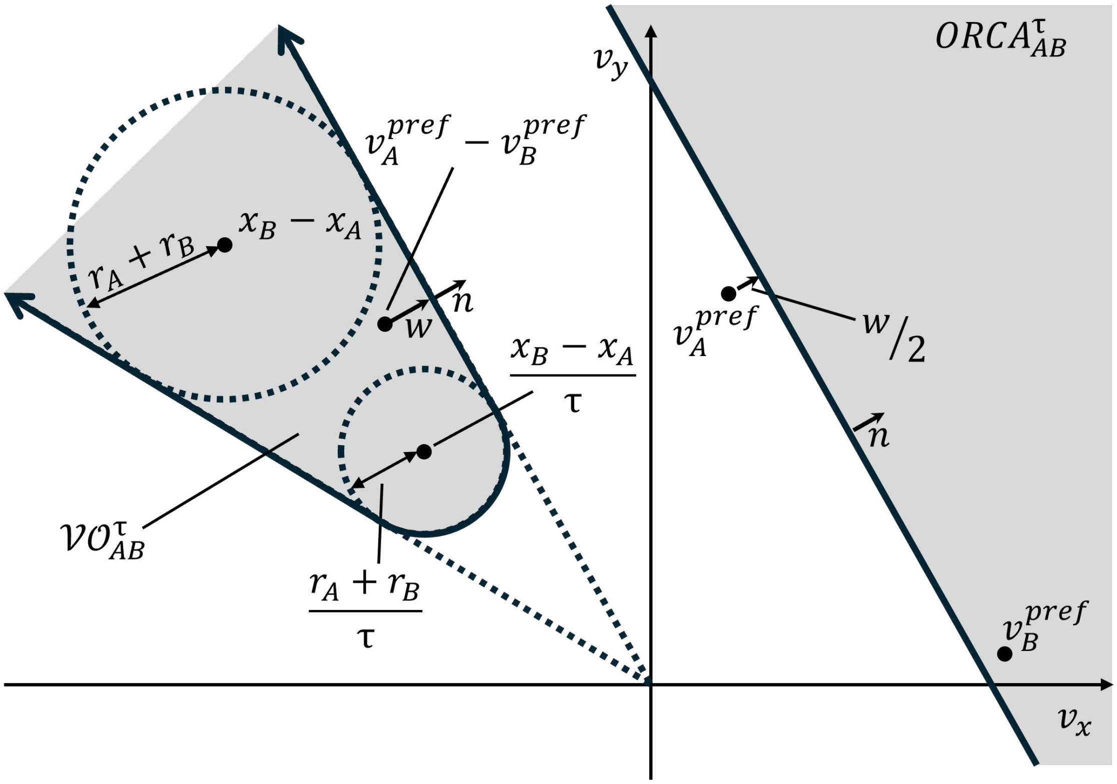

Figure 2.4: Geometry of $\mathcal{VO}_{AB}^{\tau}$, adapted from [4]

to the boundary of $\mathcal{VO}_{AB}^{\tau}$, denoted as $\partial\mathcal{VO}_{AB}^{\tau}$. The resulting vector is denoted as w,

$$w = \left(\underset{v \in \partial\mathcal{VO}_{AB}^{\tau}}{\operatorname{argmin}} \left\| v - v_{AB}^{pref} \right\| \right) - v_{AB}^{pref}. \tag{2.25}$$

Assuming that the two agents share the responsibility to avoid collisions with each other, a half-plane containing velocities that A can adopt so that no collision with B occurs before τ instants of time is then described as [4]

$$ORCA_{AB}^{\tau} = \left\{ v \;\middle|\; \left(v - \left(v_A^{pref} + \frac{1}{2} w \right) \right) \cdot n > 0 \right\}, \tag{2.26}$$

where n is the outward normal vector of $\partial\mathcal{VO}_{AB}^{\tau}$ at $v_{AB}^{pref} + w$. Note that w and n are parallel if $v_{AB}^{pref} \in \mathcal{VO}_{AB}^{\tau}$ and antiparallel otherwise. With B computing its respective half-plane of collision-free velocities in a similar manner, the boundary of $ORCA_{BA}^{\tau}$ is parallel to that of

$ORCA^{\tau}_{AB}$ but the corresponding normal vector points in the opposite direction,

$$ORCA^{\tau}_{BA} = \left\{ v \,\middle|\, \left(v - \left(v^{pref}_{B} - \frac{1}{2} w \right) \right) \cdot (-n) > 0 \right\}. \tag{2.27}$$

In multi-agent scenarios with m agents, the set of feasible velocities for A is obtained by computing a half-plane with respect to each other agent $B_1, ..., B_{m-1}$ and a disc $D(0, v^{max}_{A})$, where v^{max}_{A} is the maximum speed achievable by A. Taking the intersection of all half-planes computed by A and $D(0, v^{max}_{A})$ yields

$$ORCA^{\tau}_{A} = D(0, v^{max}_{A}) \cap \bigcap_{i=1}^{m-1} ORCA^{\tau}_{AB_i}. \tag{2.28}$$

Reference [4] specifies that because the velocity obstacle is a truncated cone, for a finite time horizon τ, the origin of the velocity space always lies outside the velocity obstacle. $ORCA^{\tau}_{A}$ will therefore not be empty if the desired velocities of all agents are set to zero.

Agent A can then compute a collision-free velocity v^{new}_{A} as

$$v^{new}_{A} = \underset{v \in ORCA^{\tau}_{A}}{\operatorname{argmin}} ||v - v^{pref}_{A}||. \tag{2.29}$$

Chapter 3

Multi-Agent Coverage Control with Non-Cooperating Swarms

3.1 Introduction

In this chapter, the scenario of multiple non-cooperating swarms that independently cover a common area is introduced. First, section 3.2 outlines the need for suitable collision avoidance strategies for coverage control with multiple swarms. Then, a motivating example is presented in section 3.3. Formal guarantees for collision avoidance when the ORCA method is used are derived in section 3.4. Furthermore, the section shows an example that visualizes the procedure of ORCA independently of coverage control. Subsequently, section 3.5 investigates how ORCA can be used to avoid collisions in coverage control scenarios with multiple non-cooperating swarms by proposing a collision avoidance algorithm. Monte Carlo simulations are presented for a specific example in section 3.6.

3.2 The Need for Collision Avoidance Strategies

Previous work [45] proved that for a single swarm of multiple agents following the Voronoi partitioning approach, the agents do not collide with each other. The reference assumes that the agents are represented as points and move toward the center of mass of their respective Voronoi cells to cover a convex area. Collisions do not occur because for a convex area all Voronoi cells take a convex shape. This results in the center of mass of a Voronoi cell always being within its boundaries. Thus, an agent directly applying its desired control input to move towards the center of mass of its Voronoi cell will always stay within the respective boundaries and does not enter the cells of other agents.

However, one limitation of the proof presented in [45] is that it considers the agents as point masses and neither incorporates their shape nor a safety zone. Moreover, when multiple non-cooperating swarms operate within a common area to provide coverage, the guarantees for collision avoidance do not hold anymore. Since Voronoi cells of agents belonging to different swarms overlap, collisions with agents from other swarms can occur, even if the agents do not leave the boundaries of their cells. Therefore, a risk of collision is present during the entire travel time. Furthermore, with the approaches introduced in sections 2.3 and 2.4, it is possible that agents belonging to different swarms aim to take identical final locations. The example presented in section 3.3 shows a scenario where this is the case. Thus, it is indispensable to incorporate suitable collision avoidance strategies. Such strategies are proposed in section 3.5.

3.3 Motivating Example

Example 3.1. *A MATLAB simulation that demonstrates an example of the coverage task executed by distinct swarms with different initial positions within a common area is performed. The density distribution that specifies the importance of coverage over the area is uniform. No collision avoidance method is incorporated. Notice that since this work considers kinematics rather than dynamics with variables such as mass, force, and inertia, all simulations presented in this thesis are shown with general units of distance and time. Two swarms, each containing four agents, are placed at the following initial positions:*

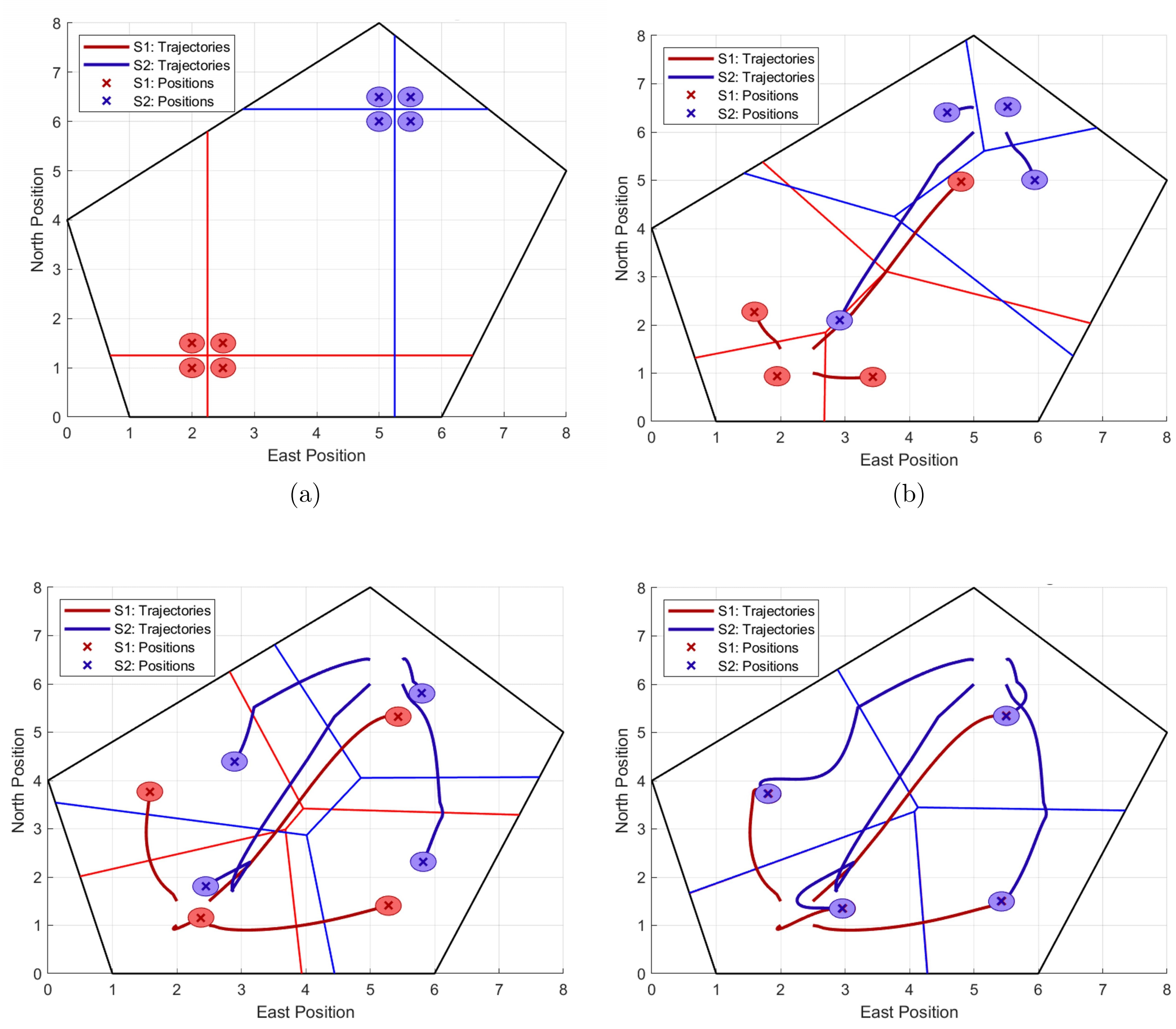

(a)

(b)

(c)

(d)

Figure 3.1: Trajectories for multi-swarm coverage (a) at time step 1 (b) after 10 time steps (c) after 50 time steps and (d) after 145 time steps.

- *Swarm 1 (S1):* $[(2,1),(2,1.5),(2.5,1),(2.5,1.5)]$,
- *Swarm 2 (S2):* $[(5,6),(5,6.5),(5.5,6),(5.5,6.5)]$.

Both groups aim to independently cover an area defined by a convex polygon with vertices at locations $[(1,0),(6,0),(8,5),(5,8),(0,4)]$. *All agents possess a circular safety zone centered at their respective positions with a radius of* 0.2 *units. The time step between computations chosen for this simulation is 0.01 units of time.*

Figure 3.1 shows the results of the simulation. In figure 3.1a, the agents and their safety zones are shown in their initial positions. The first swarm is represented in red, while the second swarm is displayed in blue. Figures 3.1b and c show the configuration of the agents as well as their traveled trajectories after 10 and 50 time steps, respectively. The final positions and complete trajectories of the agents after convergence to the centers of mass of their Voronoi cells are illustrated in figure 3.1d. Notice that in figure 3.1d the positions of the agents from the two swarms coincide, and therefore the red agents are hidden behind the blue ones. Clearly, the simulation shows a case in which both swarms converge to the same local optimum of coverage, so that agents from distinct swarms find themselves at identical final locations. This highlights the need for reliable collision avoidance.

3.4 Formal Guarantees for Collision Avoidance Using ORCA

Although reference [4] introduces a collision avoidance methodology, to the best of our knowledge, there are no theorems and proofs available in the open literature. This section will therefore establish formal guarantees for collision-free motion when ORCA is used. In addition, an example demonstrates the procedure followed by ORCA.

Theorem 3.1. *Consider two agents A and B traveling with velocities v_A and v_B, respectively. Assume that both v_A and v_B are constant for a time horizon τ. Then A and B collide before τ if and only if*

$$v_A - v_B \in \mathcal{VO}^{\tau}_{AB}, \tag{3.1}$$

where $\mathcal{VO}^{\tau}_{AB}$ is defined in (2.22) as

$$\mathcal{VO}^{\tau}_{AB} = \{v \mid \exists t \in (0, \tau] : v \in D((x_B - x_A)/t, (r_A + r_B)/t)\}. \tag{3.2}$$

Therefore, A and B do not collide if and only if

$$v_A - v_B \notin \mathcal{VO}^{\tau}_{AB}. \tag{3.3}$$

Proof. We first prove the if statement. The truncated cone of $\mathcal{VO}^{\tau}_{AB}$ (equation (3.2)) can be interpreted as

$$\mathcal{VO}^{\tau}_{AB} = \bigcup_{t\in(0,\tau]} D((x_B - x_A)/t, (r_A + r_B)/t). \tag{3.4}$$

When

$$v_{AB} = v_A - v_B \in \bigcup_{t\in(0,\tau]} D((x_B - x_A)/t, (r_A + r_B)/t), \tag{3.5}$$

it is equivalent to say that there is a $t \in (0, \tau]$ such that

$$v_{AB} \in D((x_B - x_A)/t, (r_A + r_B)/t). \tag{3.6}$$

Then,

$$\|(v_A - v_B) - (x_B - x_A)/t\| \leq (r_A + r_B)/t. \tag{3.7}$$

The positions of A and B at $t \in (0, \tau]$ are

$$\begin{aligned} x_A^{new} &= x_A + v_A t, \\ x_B^{new} &= x_B + v_B t. \end{aligned} \tag{3.8}$$

Solving (3.8) for v_A and v_B and inserting into (3.7), yields

$$\|((x_A^{new} - x_A)/t - (x_B^{new} - x_B)/t) - (x_B - x_A)/t\| \leq (r_A + r_B)/t. \tag{3.9}$$

Multiplying by t and simplifying, one obtains

$$\|x_A^{new} - x_B^{new}\| \leq r_A + r_B, \tag{3.10}$$

which indicates a collision between A and B as described in equation (2.20).

We now prove the only if statement. Note that

$$v_{AB} \notin \bigcup_{t \in (0,\tau]} D((x_B - x_A)/t, (r_A + r_B)/t) \tag{3.11}$$

is equivalent to

$$v_{AB} \notin D((x_B - x_A)/t, (r_A + r_B)/t) \tag{3.12}$$

for all $t \in (0, \tau]$. This implies that

$$\|(v_A - v_B) - (x_B - x_A)/t\| > (r_A + r_B)/t. \tag{3.13}$$

Again, we can solve (3.8) for v_A and v_B and insert the results in (3.13). After simplification,

$$\|x_A^{new} - x_B^{new}\| > r_A + r_B, \tag{3.14}$$

which means that A and B do not collide, as per equation (2.21). □

Example 3.2 illustrates the ORCA concept for a specific scenario. First, the computation of the velocity obstacles of two agents with respect to each other is shown. The second part demonstrates the identification of the corresponding half-planes. Finally, the functionality of the method with more than two agents is demonstrated.

Example 3.2. *Consider two agents A and B moving within a common area of ten by ten meters (figure 3.2). Let A and B be located at the positions $x_A = [2\ 2]^T$ meters and $x_B = [8\ 3]^T$ meters, respectively. Both agents have a radius of $r_A = r_B = 0.5$ meters. Let the goal position of agent A be at (8,8) meters and that of agent B at (2,8) meters. In this example, both agents compute their desired velocities as a vector pointing toward their goal position with the magnitude defined by their maximum speed of 0.1 meters per second. Therefore, at* *the initial time of the simulation* $t_0 = 0$ *seconds,*

$$\begin{aligned} v_A^{pref} &= [0.707\ 0.707]^T, \\ v_B^{pref} &= [-0.0768\ 0.0640]^T, \end{aligned}$$

so that

$$\begin{aligned} v_{AB}^{pref} &= [0.1475\ 0.0067]^T, \\ v_{BA}^{pref} &= [-0.1475\ \ -0.0067]^T. \end{aligned}$$

The expressions for the velocity obstacles are obtained by inserting the chosen time horizon, the positions of the agents, and their radii into equation (3.2). For $\tau = 2$ *seconds, figure 3.3 visualizes the velocity obstacle of* A *with respect to* B *(red),*

$$\mathcal{VO}_{AB}^{\tau} = \left\{ v \;\middle|\; \exists t \in (0, 2] : v \in D\left(\frac{[6\ 1]^T}{t}, \frac{1}{t} \right) \right\},$$

along with that of B *with respect to* A *(blue),*

$$\mathcal{VO}_{BA}^{\tau} = \left\{ v \;\middle|\; \exists t \in (0, 2] : v \in D\left(\frac{[-6\ \ -1]^T}{t}, \frac{1}{t} \right) \right\},$$

at $t_0 = 0$ *seconds. Clearly from figure 3.3, the* v_{AB}^{pref} *and* v_{BA}^{pref} *lie outside* $\mathcal{VO}_{AB}^{\tau}$ *and* $\mathcal{VO}_{BA}^{\tau}$*, respectively. Following Theorem 3.1, the agents will therefore not collide within the next* 2 *seconds, assuming that the desired velocities stay constant for both agents.*

In contrast, figure 3.4 shows the locations and relative desired velocities of the agents after 35 seconds. Since v_A^{pref} *and* v_B^{pref} *take the same values as at* t_0*, so do* v_{AB}^{pref} *and* v_{BA}^{pref}*. The corresponding velocity obstacles*

$$\mathcal{VO}_{AB}^{\tau} = \left\{ v \;\middle|\; \exists t \in (0, 2] : v \in D\left(\frac{[0.8364\ 0.7658]^T}{t}, \frac{1}{t} \right) \right\}$$

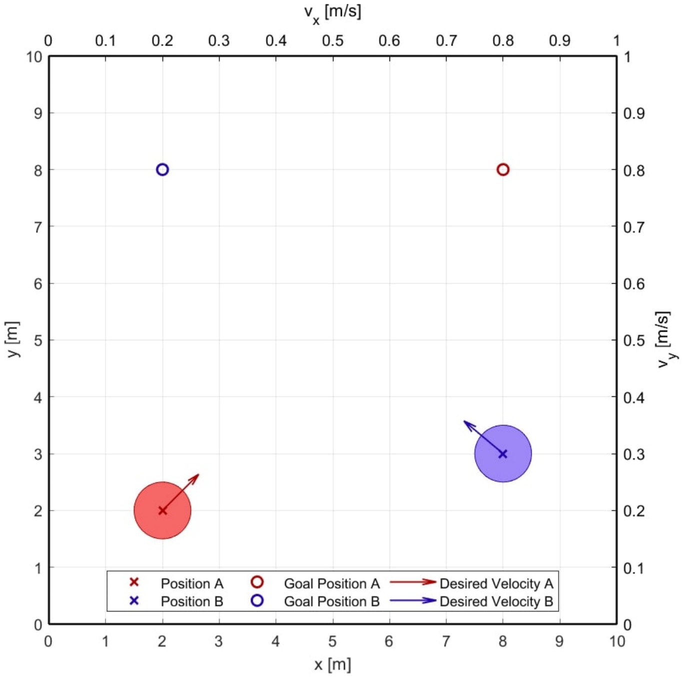

Figure 3.2: Example 3.2: Current positions, goal positions, and desired velocities of agents A and B at the initial time $t_0 = 0$ seconds

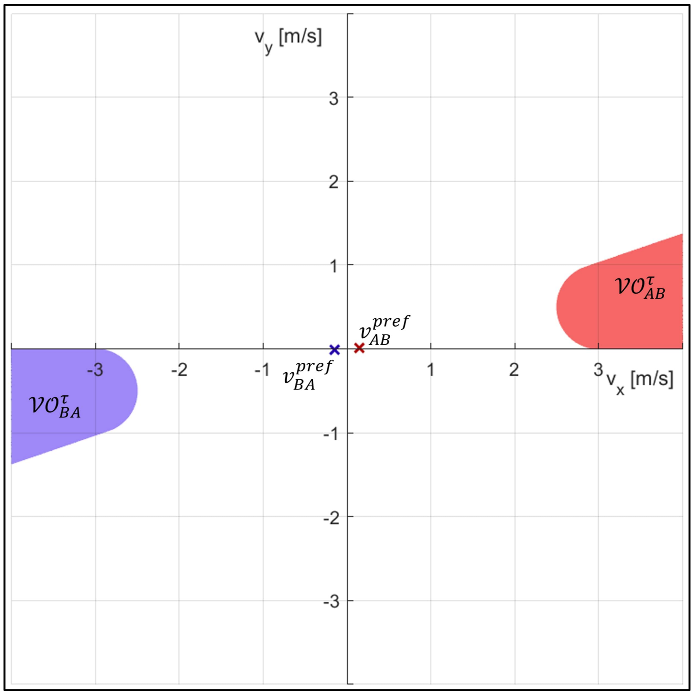

Figure 3.3: Example 3.2: Velocity obstacles of agents A and B with respect to each other and relative desired velocities at the initial time $t_0 = 0$ seconds

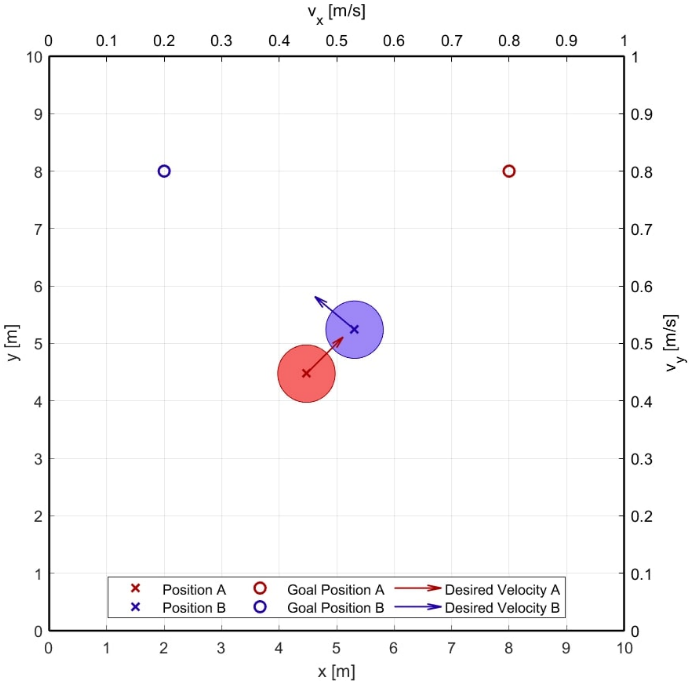

Figure 3.4: Example 3.2: Current positions, goal positions, and desired velocities of agents A and B after 36 seconds

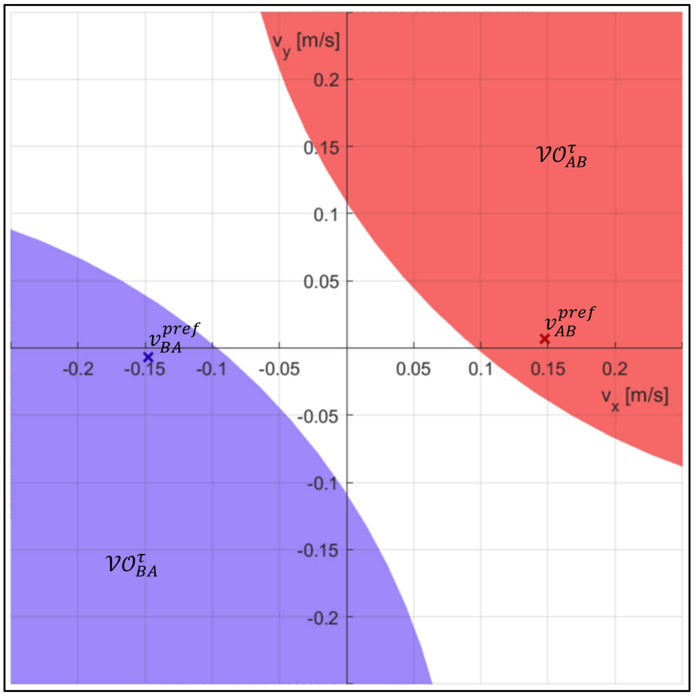

Figure 3.5: Example 3.2: Velocity obstacles of agents A and B with respect to each other and relative velocities after 36 seconds

and

$$\mathcal{VO}^{\tau}_{BA} = \left\{ v \,\middle|\, \exists t \in (0,2] : v \in D\left(\frac{[-0.8364 \;\; -0.7658]^T}{t}, \frac{1}{t} \right) \right\},$$

are depicted in figure 3.5. It is clearly visible that the v^{pref}_{AB} and v^{pref}_{BA} fall within $\mathcal{VO}^{\tau}_{AB}$ and $\mathcal{VO}^{\tau}_{BA}$, respectively. Thus, if both agents follow their desired velocities, a collision will occur within the next 2 seconds.

Theorem 3.2. *Consider an agent A moving with velocity $v^{new}_A \in ORCA^{\tau}_{AB}$ and an agent B moving with velocity $v^{new}_B \in ORCA^{\tau}_{BA}$, both computed as per equation (2.29),*

$$v^{new}_A = \underset{v \in ORCA^{\tau}_A}{argmin} \, ||v - v^{pref}_A||. \tag{3.15}$$

If both v^{new}_A and v^{new}_B are constant for a time horizon τ, then A and B do not collide before τ,i.e.,

$$v^{new}_A - v^{new}_B \notin \mathcal{VO}^{\tau}_{AB}. \tag{3.16}$$

Proof. Consider two agents A and B with desired velocities v^{pref}_A and v^{pref}_B. The half-plane of feasible velocities for agent A is the set defined in equation (2.26) whereas the half-plane of feasible velocities for B is the set defined in equation (2.27). Considering only agents A and B and using equation (3.15), A and B will choose their new velocities v^{new}_A and v^{new}_B to be the velocities closest to v^{pref}_A and v^{pref}_B contained within $ORCA^{\tau}_{AB}$ and $ORCA^{\tau}_{BA}$, respectively. Therefore,

$$v^{new}_A = v^{pref}_A + \frac{1}{2}w + an, \tag{3.17}$$

and

$$v^{new}_B = v^{pref}_B - \frac{1}{2}w - bn, \tag{3.18}$$

with $a > 0$ and $b > 0$. The new relative velocity of agent A with respect to B is

$$v^{new}_{AB} = v^{new}_A - v^{new}_B. \tag{3.19}$$

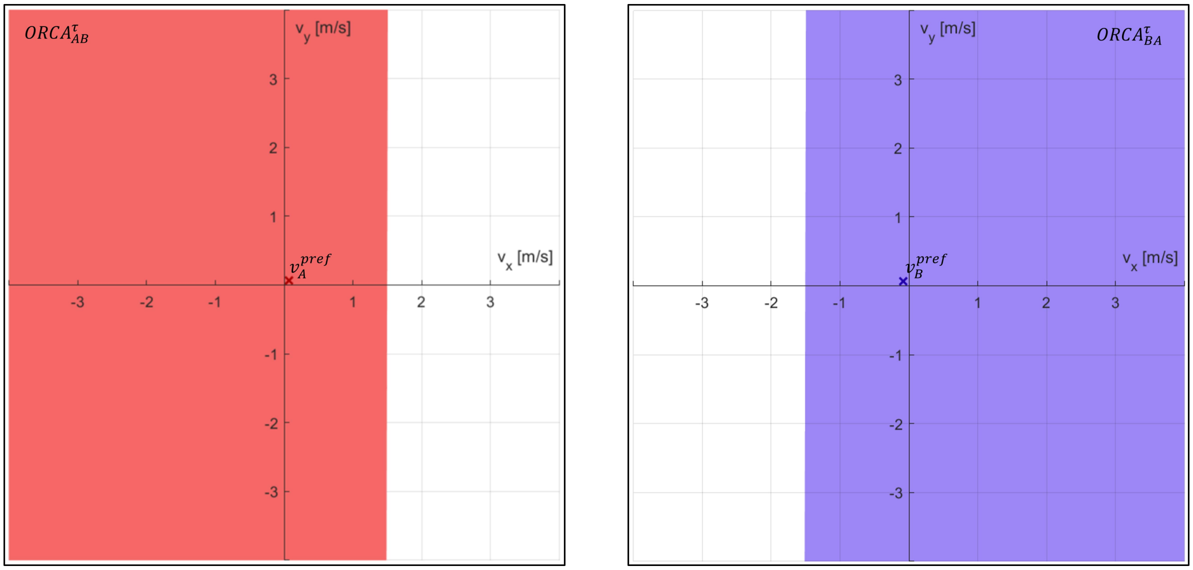

(a) (b)

Figure 3.6: Example 3.2: Half-planes of permitted velocities of (a) agent A with respect to B and (b) agent B with respect to A at the initial time $t_0 = 0$ seconds

Inserting (3.17) and (3.18) into (3.19) and simplifying yields

$$v_{AB}^{new} = v_A^{pref} - v_B^{pref} + w + (a+b)n. \tag{3.20}$$

By definition of w from equation (2.25),

$$w = \left(\underset{v \in \partial \mathcal{VO}^{\tau}_{AB}}{\operatorname{argmin}} \left\| v - v_{AB}^{pref} \right\| \right) - v_{AB}^{pref}, \tag{3.21}$$

this implies that v_{AB}^{new} is not contained within $\mathcal{VO}^{\tau}_{AB}$, i.e.

$$v_A^{new} - v_B^{new} \notin \mathcal{VO}^{\tau}_{AB}, \tag{3.22}$$

so that no collision occurs according to Theorem 3.1. □

Example 3.2 (continued)**.** *The half-planes of permitted velocities corresponding to the velocity obstacles and the desired velocities computed in figures 3.3 and 3.5 are illustrated in figures 3.6 and 3.7, respectively. Figure 3.6a shows the half-plane of permitted velocities of agent A*

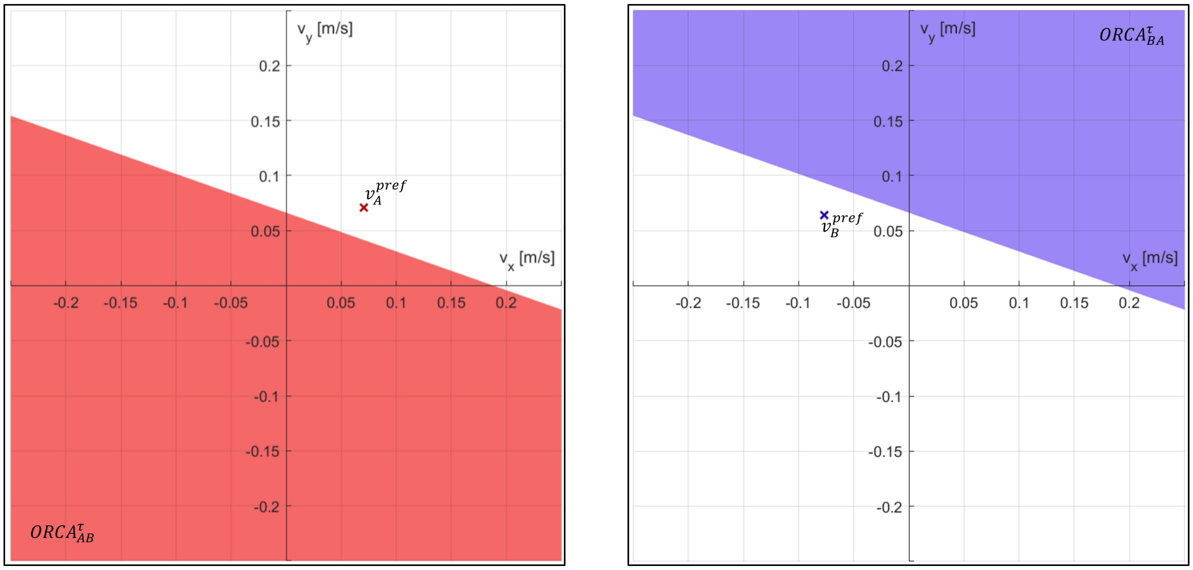

(a) (b)

Figure 3.7: Example 3.2: Half-planes of permitted velocities of (a) agent A with respect to B and (b) agent B with respect to A after 35 seconds

with respect to B at the initial time $t_0 = 0$ seconds. Its expression is obtained by inserting v_A^{pref}, w (computed using equation (3.21)), and n into equation (2.26),

$$ORCA_{AB}^{\tau} = \left\{ v \;\middle|\; \left(v - [1.4969 \; 0.0674]^T \right) \cdot [-0.9999 \; 0.0023]^T > 0 \right\}.$$

In turn, figure 3.6b depicts the half-plane of permitted velocities of agent B with respect to A at the same instant of time

$$ORCA_{BA}^{\tau} = \left\{ v \;\middle|\; \left(v - [-1.5031 \; 0.0674]^T \right) \cdot [0.9999 \;\; -0.0023]^T > 0 \right\},$$

where v_B^{pref}, w, and n are inserted into equation (2.27). It is evident from figure 3.6 that the desired velocities of both agents fall within the respective half-planes. The agents do therefore not need to adapt their velocities to avoid collisions within the next 2 seconds.

On the other hand, the half-planes of permitted velocities after 35 seconds are shown in *figures 3.7a (agent A with respect to B),*

$$ORCA^{\tau}_{AB} = \left\{ v \,\middle|\, \left(v - [0.0615 \; 0.0446]^T \right) \cdot [-0.3320 \;\; -0.9433]^T > 0 \right\},$$

and 3.7b (agent B with respect to A),

$$ORCA^{\tau}_{BA} = \left\{ v \,\middle|\, \left(v - [-0.0674 \; 0.0901]^T \right) \cdot [0.3320 \; 0.9433]^T > 0 \right\}.$$

Clearly from figure 3.7, the desired velocities of the agents do not fall within the corresponding half-planes. The agents must therefore choose new velocities in the respective half-planes of permitted velocities to avoid a collision.

Theorem 3.3. *Consider an agent A and an agent B. Let A adopt any velocity $v^{new}_A \in ORCA^{\tau}_{AB}$ and let B adopt any velocity $v^{new}_B \in ORCA^{\tau}_{BA}$. If v^{new}_A and v^{new}_B are constant for a time horizon τ, then A and B do not collide before τ, i.e.,*

$$v^{new}_A - v^{new}_B \notin \mathcal{VO}^{\tau}_{AB}. \tag{3.23}$$

Proof. Define a velocity p as

$$p = v^{pref}_A - v^{pref}_B + w \tag{3.24}$$

and a half-plane

$$\pi = \{ v \,|(v - p) \cdot n > 0 \}. \tag{3.25}$$

Then, using equations (3.24) and (3.25) and the definition of w (equation (2.25)) it can be concluded that

$$\pi \cap \mathcal{VO}^{\tau}_{AB} = \emptyset. \tag{3.26}$$

From (2.26), when choosing a new velocity $v^{new}_A \in ORCA^{\tau}_{AB}$,

$$\left(v^{new}_A - \left(v^{pref}_A + \frac{1}{2} w \right) \right) \cdot n > 0 \tag{3.27}$$

must be fulfilled. Similarly, using (2.27), v_B^{new} must satisfy

$$\left(v_B^{new} - \left(v_B^{pref} - \frac{1}{2}w\right)\right) \cdot (-n) > 0. \tag{3.28}$$

Rearranging (3.27) yields

$$v_A^{new} \cdot n > \left(v_A^{pref} + \frac{1}{2}w\right) \cdot n. \tag{3.29}$$

Moreover, we can rearrange (3.28) to obtain

$$v_B^{new} \cdot (-n) > -\left(v_B^{pref} - \frac{1}{2}w\right) \cdot n. \tag{3.30}$$

Adding (3.29) and (3.30) maintains the validity of the inequality and yields

$$v_A^{new} \cdot n + v_B^{new} \cdot (-n) > \left(v_A^{pref} + \frac{1}{2}w\right) \cdot n + \left(-\left(v_B^{pref} - \frac{1}{2}w\right) \cdot n\right), \tag{3.31}$$

which can be simplified to

$$(v_A^{new} - v_B^{new}) \cdot n > \left(v_A^{pref} - v_B^{pref} + w\right) \cdot n. \tag{3.32}$$

Using equation (3.24), we can rewrite equation (3.32) as

$$(v_A^{new} - v_B^{new}) \cdot n > p \cdot n, \tag{3.33}$$

which is equivalent to

$$(v_A^{new} - v_B^{new} - p) \cdot n > 0. \tag{3.34}$$

Therefore, from (3.25),

$$v_A^{new} - v_B^{new} \in \pi. \tag{3.35}$$

Using equation (3.26), (3.23) follows. □

Corollary 3.1. *Consider m agents operating within the same area and following the ORCA approach to avoid collisions with each other. Then an agent A choosing its new velocity $v_A^{new} \in ORCA_A^\tau$, where $ORCA_A^\tau$ is defined in equation (2.28) as*

$$ORCA_A^\tau = D(0, v_A^{max}) \cap \bigcap_{i=1}^{m-1} ORCA_{AB_i}^\tau, \tag{3.36}$$

will not collide with any other agent $B_i, i \in \{1, ..., m-1\}$, before a time horizon τ, if $v_{B_i}^{new} \in ORCA_{B_i}^\tau$, assuming that v_A^{new} and $v_{B_i}^{new}$ are constant for τ, i.e.,

$$v_A^{new} - v_{B_i}^{new} \notin \mathcal{VO}_{AB_i}^\tau, \forall i \in \{1, ..., m-1\}\,. \tag{3.37}$$

Proof. From the definition of $ORCA_A^\tau$ (equation (3.36)), assuming that v_A^{max} is finite,

$$ORCA_A^\tau \subset ORCA_{AB_i}^\tau, \forall i \in \{1, ..., m-1\}\,. \tag{3.38}$$

Therefore, $v_A^{new} \in ORCA_A^\tau$ implies that $v_A^{new} \in ORCA_{AB_i}^\tau$. From Theorem 3.3, we know that $v_A^{new} \in ORCA_{AB_i}^\tau$ and $v_{B_i}^{new} \in ORCA_{B_iA}^\tau$ leads to

$$v_A^{new} - v_{B_i}^{new} \notin \mathcal{VO}_{AB_i}^\tau, \tag{3.39}$$

which is (3.37). □

Example 3.2 (continued)**.** *Let 4 agents be located as follows,*

- *A at (5,5) meters with goal position at (1,3) meters,*
- *B_1 at (8,3) meters with goal position at (2,8) meters,*
- *B_2 at (2,3) meters with goal position at (8,6) meters,*
- *B_3 at (7,8) meters with goal position at (5,3) meters.*

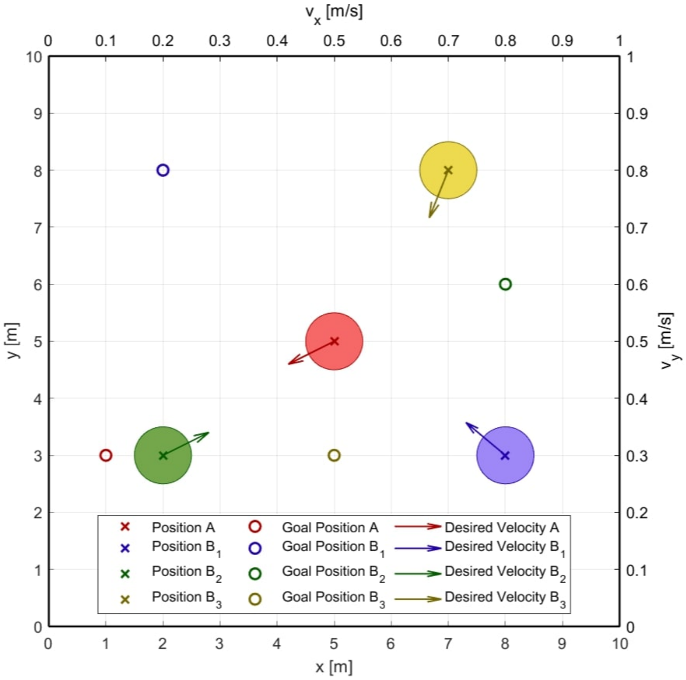

Figure 3.8: Example 3.2: Current positions, goal positions, and desired velocities of agents A, B_1, B_2, and B_3 at the initial time $t_0 = 0$ seconds

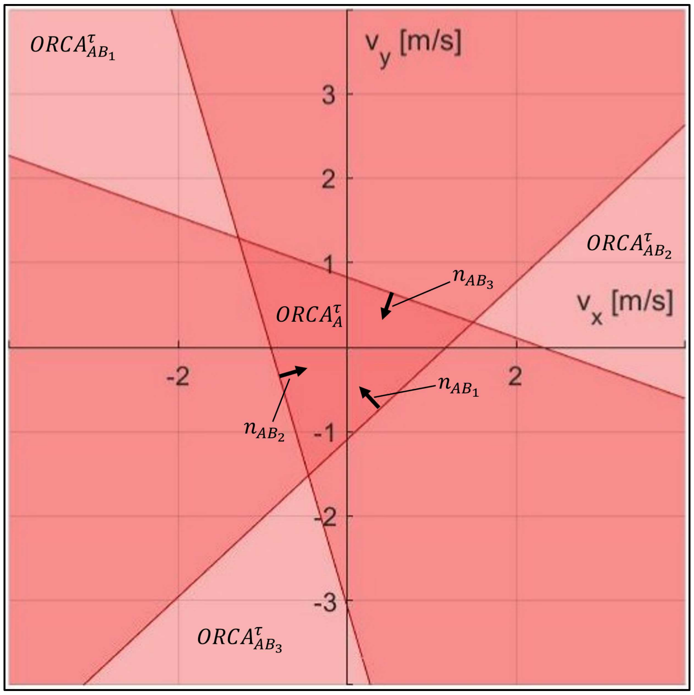

Figure 3.9: Example 3.2: Half-planes of permitted velocities of agent A with respect to each of the other agents at the initial time $t_0 = 0$ seconds

As before, the agents compute their desired velocities as a vector pointing toward their goal position with the magnitude defined by the maximum speed which is 0.1 meters per second for each agent. Figure 3.8 illustrates the scenario at the initial time $t_0 = 0$ *seconds. The half-planes of permitted velocities for agent* A *with respect to each other agent are*

$$\begin{aligned} ORCA^{\tau}_{AB_1} &= \left\{ v \,\middle|\, \left(v - [0.4759 \;\; -0.6517]^T \right) \cdot [-0.6816 \; 0.7318]^T > 0 \right\}, \\ ORCA^{\tau}_{AB_2} &= \left\{ v \,\middle|\, \left(v - [-0.8255 \;\; -0.2617]^T \right) \cdot [0.9592 \; 0.2827]^T > 0 \right\}, \\ ORCA^{\tau}_{AB_3} &= \left\{ v \,\middle|\, \left(v - [0.1984 \; 0.7568]^T \right) \cdot [-0.3380 \;\; -0.9411]^T > 0 \right\}, \end{aligned}$$

and are shown in figure 3.9. Notice that in the figure the label n_{AB_i} *indicates the normal vector corresponding to half-plane* $ORCA^{\tau}_{AB_i}$*. Clearly, choosing a velocity vector located within one half-plane does not imply the validity of the new velocity with respect to the other agents. Instead, the new velocity must be part of the intersection of all half-planes of permitted velocities, which is labeled* $ORCA^{\tau}_{A}$ *in figure 3.9.*

3.5 Algorithm for Collision-free Coverage Control with Multiple Swarms

In this section, an algorithm (algorithm 1) to incorporate collision avoidance into Voronoi-based coverage control is proposed, specifically for the case where multiple non-cooperating swarms independently aim to cover a shared area. The following assumptions are made:

1. Planar motion of the agents is assumed. For flying vehicles such as UAVs, this corresponds to the scenario where all agents operate at the same constant altitude.
2. All swarms use the same algorithm to cover the area and avoid other vehicles.
3. The computations are executed synchronously for all agents.

4. Group affiliation, as well as the radius of the circle that defines a safety zone, is known for each agent.

5. Knowledge regarding the locations of all other agents within the same swarm can be obtained through communication between vehicles.

6. Knowledge regarding the locations of all agents from other swarms can be obtained using sensors.

Notice that, considering that agents from different swarms do not collaborate, assumption 6 may seem stringent at first. However, an example of a setup to obtain the positions of agents from other swarms is the sensing of their distance from multiple agents belonging to the same swarm. Based on these measurements and respective computations, the locations of agents from other swarms can be estimated.

Algorithm 1 Computation of a Collision-Free Velocity for an Agent in a Multi-Swarm Coverage Control Scenario

```
Input: $X, Q$
Output: $v_{i,j}^{new}$
$X \leftarrow \text{update}(X)$;
$x_{i,j} \leftarrow X_j(i)$;
$Edges_j, Vertices_j \leftarrow \text{voronoi}(X_j, Q)$;
$CM_{V_{i,j}} \leftarrow \text{centerOfMass}(Edges_j(i), Vertices_j(i))$;
$v_{i,j}^{pref} \leftarrow \text{desiredVelocity}(CM_{V_{i,j}}, x_{i,j}, k_{i,j})$;
for all $X_l \subset X$, $l = \{1, ..., N\}$ do
    for all $x_{k,l} \in X_l, \forall\, (k,l) \neq (i,j), k = \{1, ..., m\}$ do
        $Edges_l, Vertices_l \leftarrow \text{voronoi}(X_l, Q)$;
        $CM_{V_{k,l}} \leftarrow \text{centerOfMass}(Edges_l(k), Vertices_l(k))$;
        $\hat{v}_{k,l}^{pref} \leftarrow \text{desiredVelocity}(CM_{V_{k,l}}, x_{k,l}, \hat{k}_{k,l})$;
        $\mathcal{VO}_{(i,j)(k,l)}^{\tau} \leftarrow \text{velocityObstacle}(x_{i,j}, x_{k,l}, r_{i,j}, r_{k,l}, \tau)$;
        $ORCA_{(i,j)(k,l)}^{\tau} \leftarrow \text{halfplane}(\mathcal{VO}_{(i,j)(k,l)}^{\tau}, v_{i,j}^{pref}, \hat{v}_{k,l}^{pref})$;
    end for
    $ORCA_{(i,j)(l)}^{\tau} \leftarrow \bigcap_{k=1}^{m} ORCA_{(i,j)(k,l)}^{\tau}$;
end for
$ORCA_{i,j}^{\tau} \leftarrow D(0, v_{i,j}^{max}) \cap \bigcap_{l=1}^{N-1} ORCA_{(i,j)(l)}^{\tau}$;
$v_{i,j}^{new} \leftarrow \text{newVelocity}(ORCA_{i,j}^{\tau})$;
return $v_{i,j}^{new}$
```

Algorithm 1 modifies ORCA to incorporate it into Voronoi-based coverage control to avoid collisions between vehicles belonging to N different swarms. For agents with first-order dynamics introduced in sections 2.3 and 2.4, the control input is a velocity vector that an agent i aims to adopt. We therefore set $v_i^{pref} = u_i$. With ORCA operating in the velocity space, the algorithm uses ORCA to modify the desired control inputs of the agents and obtain a new collision-free velocity v_i^{new} for each agent.

The algorithm is executed by each agent individually at each time step. The notation of $x_{i,j}$ and $v_{i,j}$ indicates the position and velocity of the i^{th} agent belonging to the j^{th} swarm, respectively. X stands for a set that contains the positions of all agents, while $X_j \subset X$ includes only those belonging to swarm j. After updating the positions of all agents including its own for the current time step (lines 1,2 in algorithm 1), agent i of swarm j computes the Voronoi tessellation generated by the members of its swarm and calculates the location of the center of mass of its Voronoi cell (lines 3,4). Subsequently (line 5), the computation of its desired control input velocity follows. This is done by obeying the coverage control approach introduced in equation (2.9) and repeated here for convenience

$$v_{i,j}^{pref} = u_{i,j} = k_{i,j}(CM_{V_{i,j}} - x_{i,j}), \tag{3.40}$$

where $k_{i,j}$ can be selected as

$$k_{i,j} = \sqrt{\frac{s_{i,j}}{r_{i,j}}} \tag{3.41}$$

to obtain the control input described in equation (2.13) that takes energy-efficiency into account. Note that in this step, the avoidance of potential collisions with other agents is not yet addressed.

Corrections to the preferred velocity are made using ORCA to avoid collisions with other agents (lines 6-17). For each swarm, the Voronoi tessellation over the area is computed along with the centers of mass of the Voronoi cells (lines 8,9). Estimates of the desired velocities of the agents are obtained using assumption 2 (line 10).

The truncated Velocity Obstacle cones with respect to the other agents are computed in line 11. The corresponding half-planes are inferred and intersected with each other and with a disc of radius $v_{i,j}^{max}$ centered at the origin of the velocity space to obtain the set of permitted velocities (lines 12-16). Finally, agent i, j chooses its new velocity from the set of permitted velocities that do not result in collision with other agents (line 17). This is done using equation (2.29).

3.6 Simulations

To validate the algorithm proposed in section 3.5, simulations with multiple non-cooperating swarms independently covering a common area were run and are presented in this section. The section is divided into two parts. First, the setup and results of Monte Carlo simulations are shown, before a specific example is presented. All simulations are performed in MATLAB R2019a on a laptop featuring 16 GB of RAM and an Intel Core i7-1255U CPU with base speed 1.7 GHz.

Consider the same area Q as in Example 3.1 with the vertices of the boundaries located at $[(1,0),(6,0),(8,5),(5,8),(0,4)]$. To demonstrate that the agents do not collide, when the proposed algorithm is implemented, Monte Carlo simulations of 100 repetitions were executed for different initial positions of two swarms, each consisting of four agents. Notice that all algorithms proposed in this thesis are general for any number of swarms. However, for simplicity, only simulations with two swarms are presented. Notice also that the swarms do not need to contain the same number of agents. For all simulations presented in this thesis, the desired velocity for each agent is computed using equation (2.13) with $s_{i,j} = r_{i,j} = 1, \forall i \in \{1, ..., m\}, \forall j \in \{1, ..., N\}$. The time step between computations is chosen to be 0.01 units of time. For collision avoidance, the time horizon τ is chosen to be one time step. This implies that the computed Velocity Obstacle cones include all velocities that result in collision during the next time step. Notice that choosing the time horizon τ is a

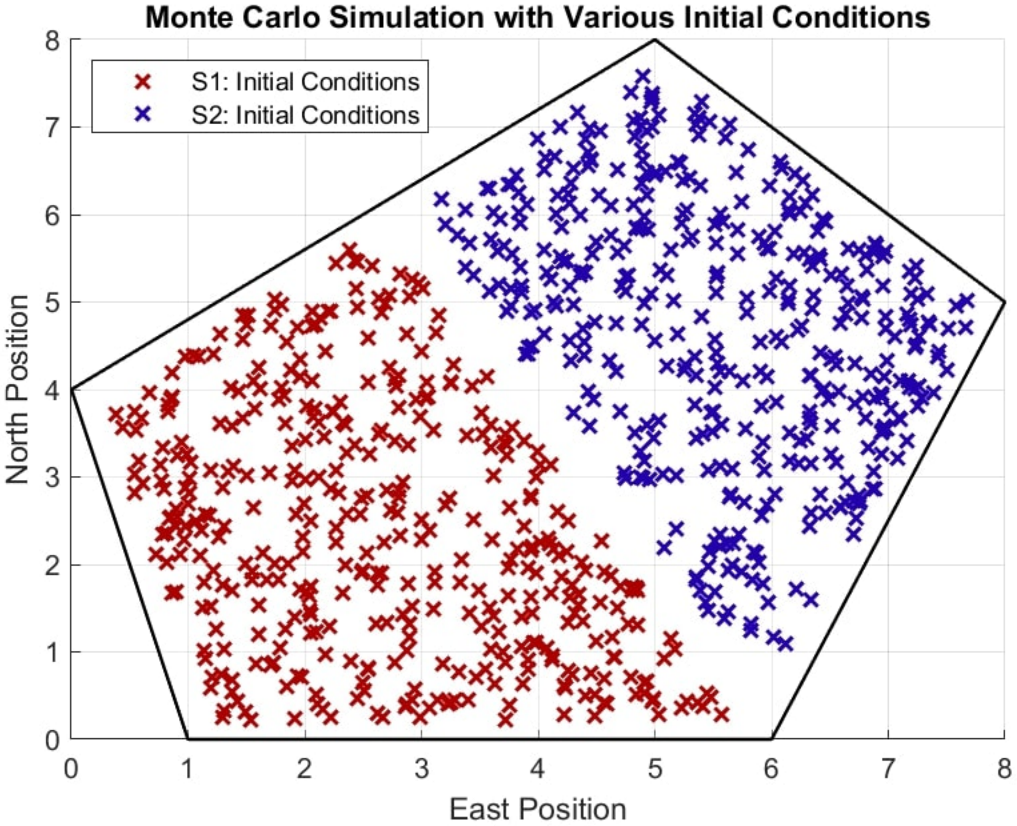

Figure 3.10: Initial positions of agents in Monte Carlo simulations of 100 repetitions

trade-off. On the one hand, choosing a large time horizon means that collision-free motion can be guaranteed for a long time without recomputation of new velocity obstacles and half-planes of permitted velocities. However, it is assumed that the agents keep their velocities constant during the chosen time horizon, which in real-world scenarios may require choosing a smaller time horizon.

For each repetition of the simulation, the initial locations of the four agents of swarm 1 are randomly chosen from an area $Q_{S1} \subset Q$ with the vertices of its boundaries at $[(1,0),(6,0),(2.5,6),(0,4)]$. Similarly, the initial locations of the four agents of swarm 2 are randomly chosen from an area $Q_{S2} \subset Q$ that has the vertices of its boundaries at $[(0,6),(8,5),(5,8),(2.5,6)]$. This ensures that at the beginning of each repetition of the simulation, at least one part of Q is not well covered by each swarm. To achieve coverage over the entirety of Q, the trajectories of the agents will therefore be comparatively long. This

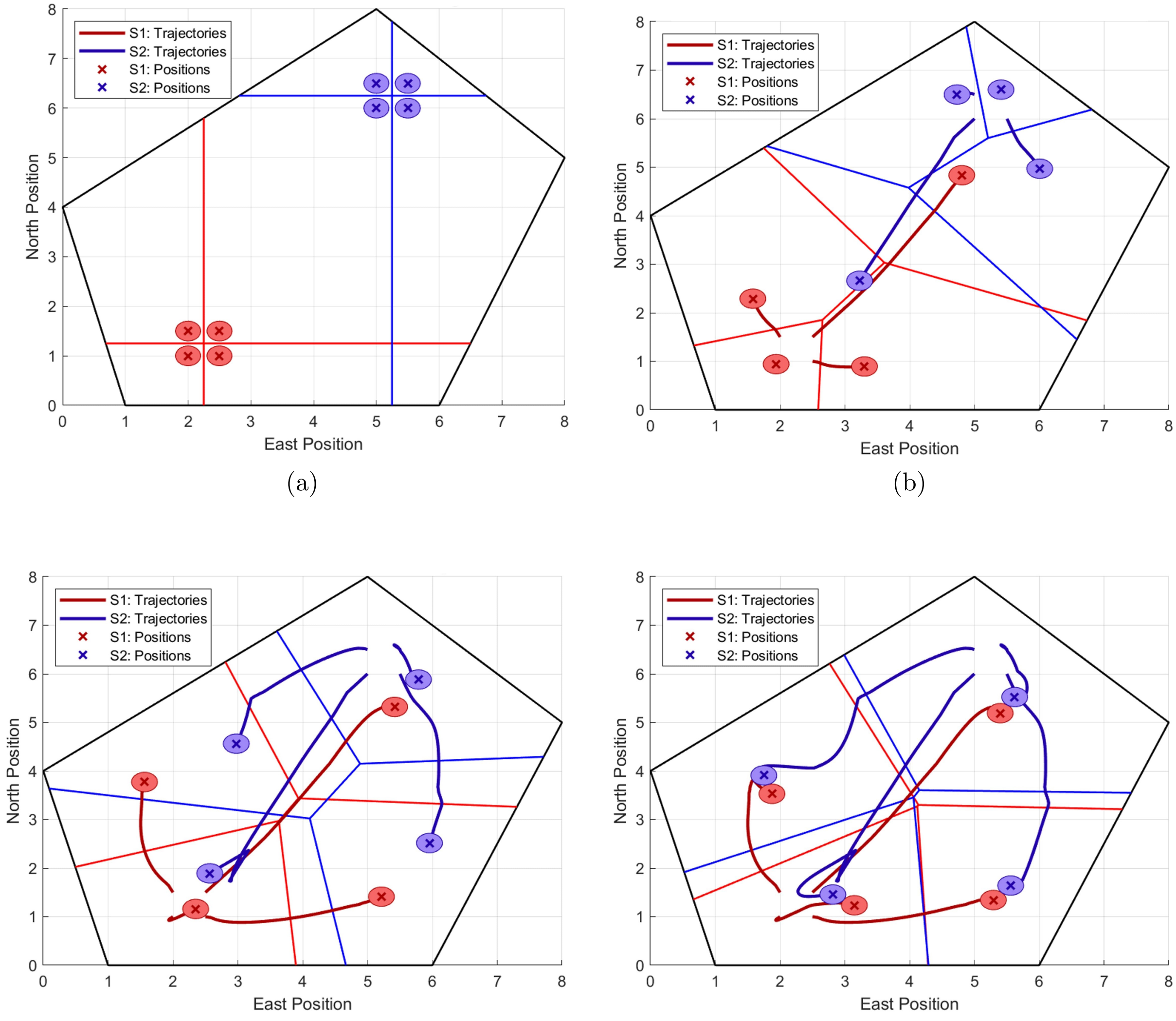

(a)

(b)

(c)

(d)

Figure 3.11: Simulation of coverage control with two non-cooperating swarms with collision avoidance showing the trajectories and positions of the agents of swarm 1 (S1) and swarm 2 (S2) (a) at the first time step (b) after 10 time steps (c) after 50 time steps (d) after convergence to their final positions.

increases the likelihood of encounters with agents from the other swarm. It is ensured that each agent always starts at a collision-free distance from each other agent (at least the sum of its own and the other agent's radius) and at a minimum distance from the boundaries of Q. All simulated sets of initial positions are visualized in figure 3.10.

In 100 repetitions of the simulation with random initial positions of the agents as described, no collision occurred. An illustration of a specific example is demonstrated in Example 3.3.

Example 3.3. *This example illustrates the coverage task executed by distinct swarms of four agents each within a common area using the proposed algorithm, where collision avoidance is implemented. Suppose the same conditions as in Example 3.1, with a uniform density distribution over the area with the vertices of its boundary at* $[(1,0),(6,0),(8,5),(5,8),(0,4)]$. *The agents of the two swarms are placed at the following positions:*

- *Swarm 1 (S1):* $[(2,1),(2,1.5),(2.5,1),(2.5,1.5)]$,
- *Swarm 2 (S2):* $[(5,6),(5,6.5),(5.5,6),(5.5,6.5)]$.

The radii of the safety zones of all agents are 0.2 *units. The time step between computations is chosen to be 0.01 units of time, and the time horizon* τ *is one time step. The desired velocity*

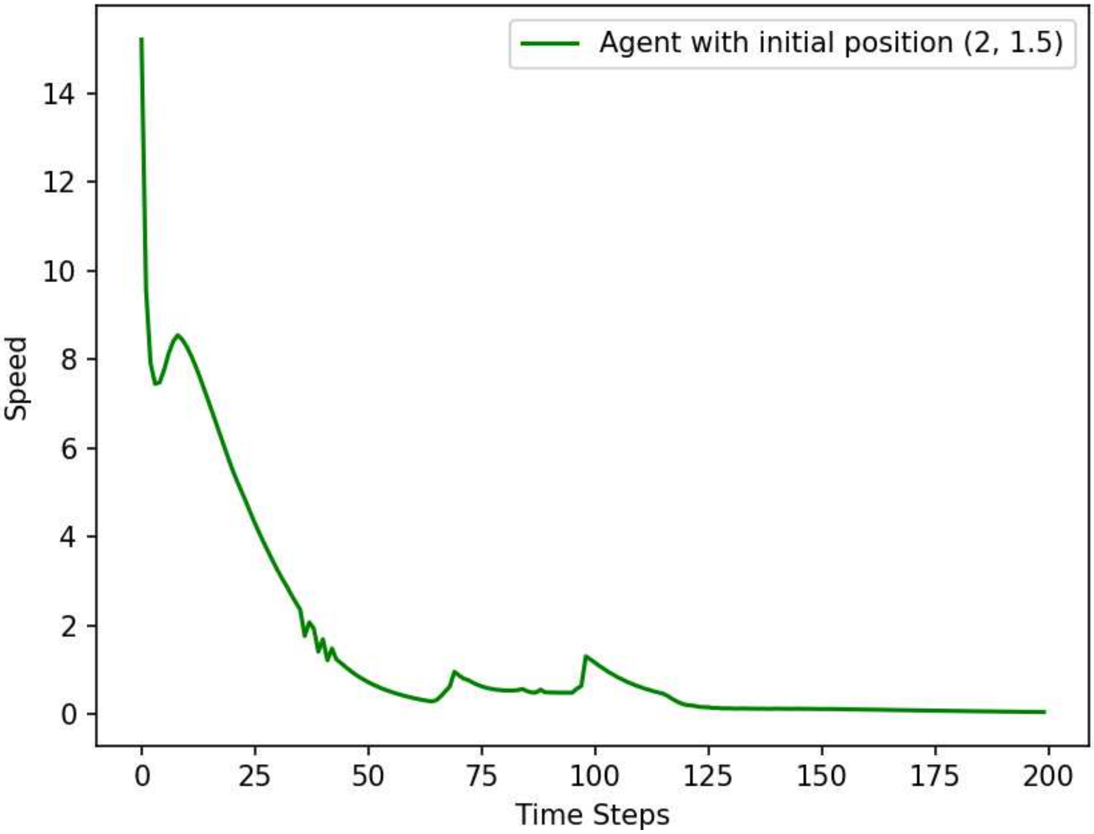

Figure 3.12: Plot of the speed of the agent initially located at (2, 1.5)

for each agent is computed using equation (2.13) with $s_{i,j} = r_{i,j} = 1, \forall i \in \{1, ..., m\}, \forall j \in \{1, ..., N\}$.

The results obtained are depicted in figure 3.11. The agents of both swarms are shown in their initial locations in figure 3.11a. After 10 time steps (figure 3.11b) and 50 time steps (figure 3.11c), the trajectories traveled by the agents are still similar to those observed after the same number of time steps in Example 3.1. Notice that despite the trajectories appearing to cross each other, no collisions occurred. This is because the agents reached these intersections at different points in time. As the agents approach their final positions (figure 3.11d), the differences between the simulation without obstacle avoidance in Example 3.1 and the simulations with obstacle avoidance are clearly visible. Instead of reaching the centers of mass of their Voronoi cells, the agents from different swarms aim to converge to the same final positions and compete for their respective spots to achieve maximum coverage. Yet, collisions do not occur, which supports the suitability of the proposed algorithm.

Figure 3.12 visualizes the speed of the agent that is initially located at position (2, 1.5). It is clearly visible that the agent first moves at high speed and then decelerates as it approaches the center of mass of its Voronoi cell.

Chapter 4

Multi-Swarm Coverage Control with Bounded Disturbance Measurement Uncertainty

4.1 Introduction

This chapter introduces a collision avoidance methodology for multi-agent systems in the presence of bounded disturbance measurement uncertainties. First, the uncertainties considered in this chapter are described and modeled in section 4.2. Section 4.3 introduces the proposed methodology and formalizes the results through theorems and proofs guaranteeing collision-free motion. The method is then applied to multi-swarm coverage control as introduced in chapter 3. This is done through an algorithm proposed in section 4.4. MATLAB simulations showing an example for collision-free motion in multi-swarm coverage control are presented in section 4.5 to validate the functionality of the proposed collision avoidance methodology and the corresponding algorithm.

4.2 Modeling of Disturbances and Measurement Uncertainty

Consider a first-order system where a velocity control input is applied to an agent i operating in the presence of a disturbance. Denote the velocity of the disturbance at the location of i as $v_{d(i)}(t)$. Then, the dynamics are

$$\begin{aligned} \dot{x}_i &= v_i, \\ v_i &= u_i + v_{d(i)}(t). \end{aligned} \tag{4.1}$$

Although technologies exist that measure disturbance velocities at a specific location, uncertainties in the measurements need to be accounted for. In this work, the measured disturbance velocity at the location of i is denoted as $v_{d(i)}^{meas}(t)$. It is described by the real disturbance velocity plus an additive sensor bias $b_{d(i)}$ and time-dependent noise $e_{d(i)}(t)$,

$$v_{d(i)}^{meas}(t) = v_{d(i)}(t) + b_{d(i)} + e_{d(i)}(t). \tag{4.2}$$

It is assumed that an estimate $\hat{b}_{d(i)}$ for $b_{d(i)}$ is available. We will describe the deviation of $\hat{b}_{d(i)}$ from $b_{d(i)}$ as

$$\delta b_{d(i)} = b_{d(i)} - \hat{b}_{d(i)}. \tag{4.3}$$

To obtain an estimate $\hat{v}_{d(i)}(t)$ for the disturbance velocity based on the measured value and the estimated sensor bias, let

$$\hat{v}_{d(i)}(t) = v_{d(i)}^{meas}(t) - \hat{b}_{d(i)}. \tag{4.4}$$

Inserting $v_{d(i)}^{meas}(t)$ as defined in equation (4.2) into equation (4.4) yields

$$\hat{v}_{d(i)}(t) = v_{d(i)}(t) + b_{d(i)} + e_{d(i)}(t) - \hat{b}_{d(i)}, \tag{4.5}$$

which using equation (4.3) leads to

$$\hat{v}_{d(i)}(t) = v_{d(i)}(t) + \delta b_{d(i)} + e_{d(i)}(t). \tag{4.6}$$

Let

$$\xi_{d(i)}(t) = \delta b_{d(i)} + e_{d(i)}(t). \tag{4.7}$$

It is assumed that

$$\xi_{d(i)}(t) \in \varepsilon_i(z), \tag{4.8}$$

where

$$\varepsilon_i(z) = \left\{ z \,\middle|\, z^T P z \leq 1 \right\} \tag{4.9}$$

for some given $P = P^T \geq 0$ and $z = [v_x \; v_y \; 1]^T$.

Equations (4.6) and (4.7) yield

$$\hat{v}_{d(i)}(t) = v_{d(i)}(t) + \xi_{d(i)}(t). \tag{4.10}$$

Solving (4.10) for $\xi_{d(i)}(t)$ yields

$$\xi_{d(i)}(t) = \hat{v}_{d(i)}(t) - v_{d(i)}(t). \tag{4.11}$$

Given a desired velocity v_i^{pref} that is to be adopted, we will now design a velocity control input u_i that counteracts external disturbances based on their bounds. Assuming that sufficient control input to counteract these disturbances can always be achieved, consider

$$u_i = v_i^{pref} - \hat{v}_{d(i)}(t). \tag{4.12}$$

Inserting (4.12) into (4.1), we obtain

$$v_i = v_i^{pref} + v_{d(i)}(t) - \hat{v}_{d(i)}(t). \tag{4.13}$$

Using (4.11) and (4.13),

$$v_i = v_i^{pref} - \xi_{d(i)}(t). \tag{4.14}$$

The next section will address the effects of $\xi_{d(i)}(t)$ by computing a new collision-free velocity v_i^{new} based on v_i^{pref} and ε_i.

4.3 Collision Avoidance with Measurement Uncertainty

In this section, a modification of the ORCA methodology is introduced to account for bounded disturbance measurement uncertainty and guarantee collision-free motion. As in the previous chapter, we will use the alphabet to identify agents, i.e., $i = A, B, ...$, to be consistent with the notation used in reference [4] as presented in section 2.6.

Assume that the disturbance velocity field across an area is measured and communicated to all agents moving within the area. The velocity obstacle $\mathcal{VO}_{AB}^{\tau}$ is computed by equation (2.22) and repeated here for convenience,

$$\mathcal{VO}_{AB}^{\tau} = \{v \mid \exists t \in (0, \tau] : v \in D((x_B - x_A)/t, (r_A + r_B)/t)\}. \tag{4.15}$$

Subsequently, the desired relative velocity of agent A with respect to agent B is calculated as

$$v_{AB}^{pref} = v_A^{pref} - v_B^{pref}. \tag{4.16}$$

When disturbance measurement uncertainty is present, the ellipses bounding the uncertainty at the locations where agents A and B are located are ε_A and ε_B, respectively, and are described by (4.9). In that case, unlike the original ORCA approach, it is not sufficient that

v_{AB}^{pref} be outside $\mathcal{VO}_{AB}^{\tau}$. Instead, the Minkowski sum of ε_A and ε_B is computed as

$$\varepsilon_{AB}^{sum} = \varepsilon_A + \varepsilon_B = \{\eta_A + \eta_B \mid \eta_A \in \varepsilon_A, \eta_B \in \varepsilon_B\}, \tag{4.17}$$

and the resulting set ε_{AB}^{sum} is translated by v_{AB}^{pref}, which yields

$$\overline{\varepsilon_{AB}^{sum}} = \varepsilon_{AB}^{sum} + v_{AB}^{pref}. \tag{4.18}$$

A visual representation of ε_A with semi-major axis 2.5, semi-minor axis 0.8, angle of rotation 15°, ε_B with semi-major axis 1.8, semi-minor axis 1, angle of rotation 155°, and $\overline{\varepsilon_{AB}^{sum}}$ is shown in figure 4.1 for $v_{AB}^{pref} = [-3 \;\; 3]^T$.

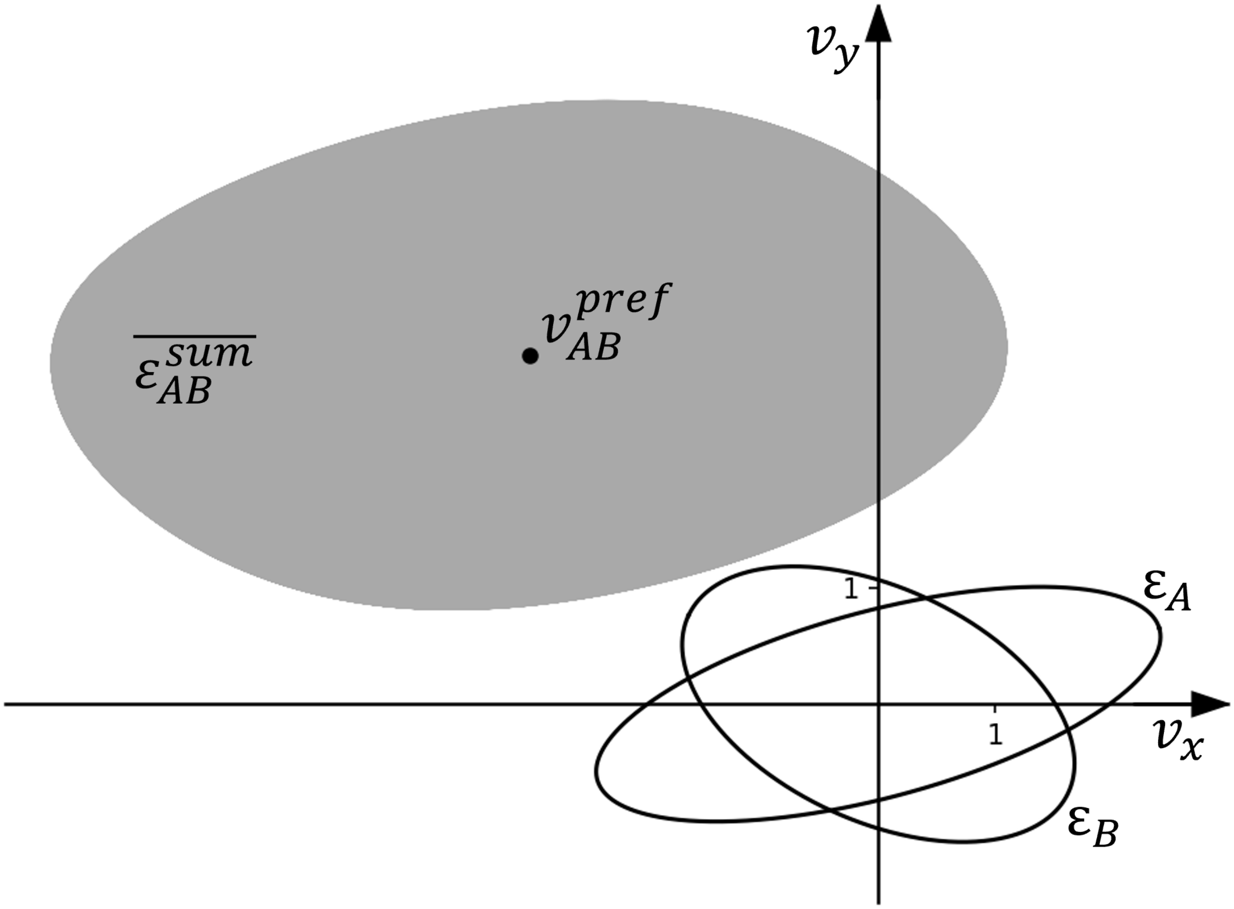

Figure 4.1: Visualization of ε_A, ε_B, and $\overline{\varepsilon_{AB}^{sum}}$

Theorem 4.1. *Assume that the constraint (4.8) is satisfied for both $\xi_{d(A)}$ and $\xi_{d(B)}$. If the agents A and B apply control inputs u_A and u_B as defined in equation (4.12) with i replaced by A and B, respectively, based on given desired velocities v_A^{pref} and v_B^{pref}, then*

$$v_A - v_B \in \overline{\varepsilon_{AB}^{sum}}, \tag{4.19}$$

where v_A and v_B are given by equation (4.14) with i replaced by A and B, respectively.

Proof. From equation (4.14) with i replaced by A and B, respectively, we can write

$$\begin{aligned} v_A &= v_A^{pref} - \xi_{d(A)}, \\ v_B &= v_B^{pref} - \xi_{d(B)}. \end{aligned} \tag{4.20}$$

Subtracting v_B from v_A yields

$$v_A - v_B = v_A^{pref} - \xi_{d(A)} - \left(v_B^{pref} - \xi_{d(B)}\right), \tag{4.21}$$

which using equation (4.16) can be rewritten as

$$v_A - v_B = -\xi_{d(A)} + \xi_{d(B)} + v_{AB}^{pref}. \tag{4.22}$$

Since $\xi_{d(A)} \in \varepsilon_A$ and $\xi_{d(B)} \in \varepsilon_B$ from equation (4.8),

$$-\xi_{d(A)} + \xi_{d(B)} \in -\varepsilon_A + \varepsilon_B, \tag{4.23}$$

where

$$-\varepsilon_A = \varepsilon_A \tag{4.24}$$

due to ε_A being symmetric about the origin. Adding v_{AB}^{pref} on both sides, we obtain

$$-\xi_{d(A)} + \xi_{d(B)} + v_{AB}^{pref} \in -\varepsilon_A + \varepsilon_B + v_{AB}^{pref}. \tag{4.25}$$

Therefore, from equation (4.22) and (4.25),

$$v_A - v_B \in -\varepsilon_A + \varepsilon_B + v_{AB}^{pref}. \tag{4.26}$$

Using (4.24) allows us to rewrite equation (4.26) as

$$v_A - v_B \in \varepsilon_A + \varepsilon_B + v_{AB}^{pref}. \tag{4.27}$$

Equations (4.17), (4.18), and (4.27) yield (4.19). □

Corollary 4.1. *Let A and B apply their control inputs u_A and u_B as defined in equation (4.12) with i replaced by A and B, respectively, based on given desired velocities v_A^{pref} and v_B^{pref}. Assume that v_A^{pref} and v_B^{pref} are constant for a time horizon τ and that the constraint (4.8) is satisfied for both $\xi_{d(A)}$ and $\xi_{d(B)}$. Then A and B will not collide before τ units of time if*

$$\overline{\varepsilon_{AB}^{sum}} \cap \mathcal{VO}_{AB}^{\tau} = \emptyset. \tag{4.28}$$

Proof. Using Theorem 4.1 we know that

$$v_A - v_B \in \overline{\varepsilon_{AB}^{sum}}. \tag{4.29}$$

Moreover, Theorem 3.1 states that a collision between A and B happens if and only if

$$v_A - v_B \in \mathcal{VO}_{AB}^{\tau}. \tag{4.30}$$

Thus, no collision occurs if and only if

$$v_A - v_B \notin \mathcal{VO}_{AB}^{\tau}, \tag{4.31}$$

which is the case when (4.28) is satisfied. □

Define

$$p = \underset{v \in \partial \mathcal{VO}_{AB}^{\tau}}{\operatorname{argmin}} \left\| v - v_{AB}^{pref} \right\|, \tag{4.32}$$

and let n be the outward normal vector of $\partial \mathcal{VO}_{AB}^{\tau}$ at p. Define

$$d = p - v_{AB}^{pref}. \tag{4.33}$$

Then d and n are collinear, i.e.,

$$d \parallel n \perp \partial \mathcal{VO}_{AB}^{\tau}. \tag{4.34}$$

Let

$$\pi = \left\{ v \,|(v - p) \cdot n > 0 \right\}. \tag{4.35}$$

Then

$$\pi \cap \mathcal{VO}_{AB}^{\tau} = \emptyset. \tag{4.36}$$

As a result of Corollary 4.1, we determine a vector w that translates $\overline{\varepsilon_{AB}^{sum}}$ outside of $\mathcal{VO}_{AB}^{\tau}$. Using (4.36) this is achieved by translating $\overline{\varepsilon_{AB}^{sum}}$ into π. We therefore solve

$$w = \begin{pmatrix} \underset{\bar{w}}{\operatorname{argmin}} \|\bar{w}\| \\ \\ \text{s.t.} \left(\overline{\varepsilon_{AB}^{sum}} + \bar{w} \right) \in \pi \end{pmatrix}, \tag{4.37}$$

or, equivalently,

$$w = \left[(p - x^*) \cdot n \right] \cdot n, \tag{4.38}$$

where

$$x^* = \begin{pmatrix} \min n^T x \\ \\ \text{s.t.} x \in \overline{\varepsilon_{AB}^{sum}} \end{pmatrix}. \tag{4.39}$$

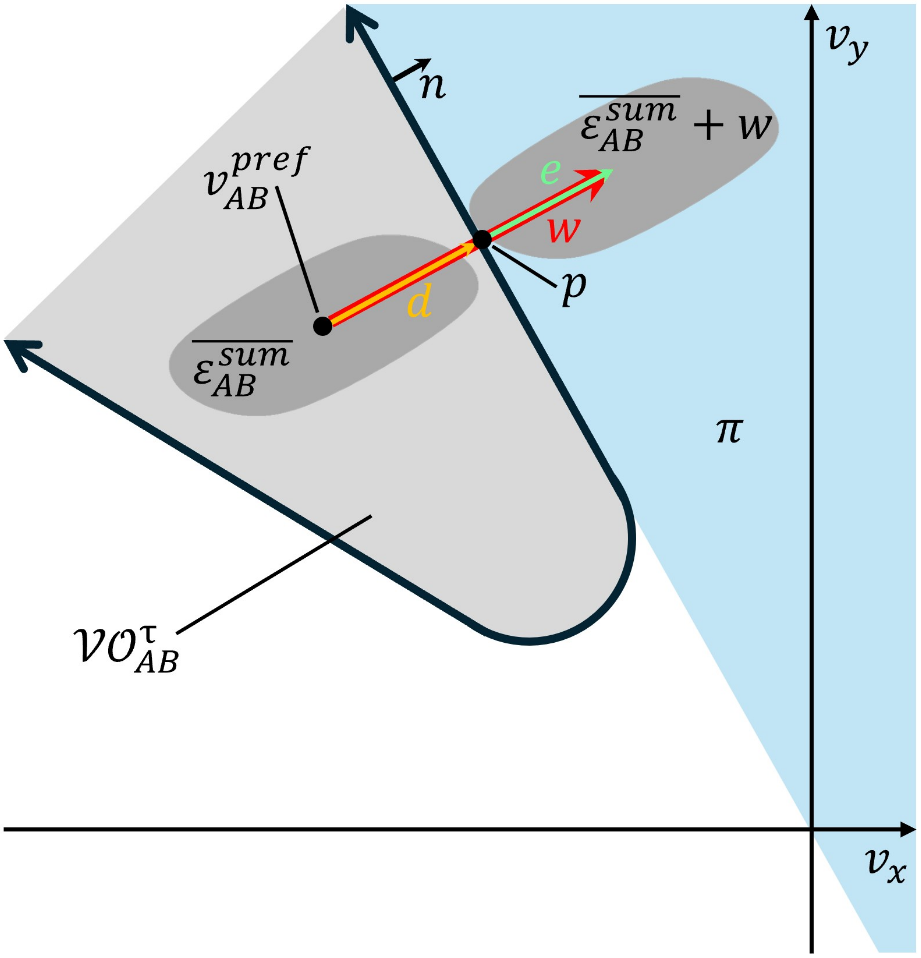
v_y
n
$\overline{\varepsilon_{AB}^{sum}} + w$
v_{AB}^{pref}
e
w
p
d
$\overline{\varepsilon_{AB}^{sum}}$
π
$\mathcal{VO}_{AB}^{\tau}$
v_x

Figure 4.2: Visualization of π

Theorem 4.2. *([46], page 46) Suppose C and D are nonempty disjoint convex sets, i.e., $C \cap D = \emptyset$. Then there exist $a \neq 0$ and b such that $a^T x \leq b$ for all $x \in C$ and $a^T x \geq b$ for all $x \in D$. In other words, the affine function $a^T x - b$ is nonpositive on C and nonnegative on D. The hyperplane $\left\{x \,\middle|\, a^T x = b\right\}$ is called a separating hyperplane for the sets C and D, or is said to separate the sets C and D.*

Note that π is the upper half-space of the hyperplane that separates $\overline{\varepsilon_{AB}^{sum}} + w$ from $\mathcal{VO}_{AB}^{\tau}$. A visualization of w is given in figure 4.2. The translation vector w is then used to define $ORCA_{AB}^{\tau}$ by equation (2.26). After obtaining the half-planes with respect to all other agents, A computes a set of collision-free velocities as in equation (2.28). The new velocity is obtained using equation (2.29).

Theorem 4.3. *Let A and B apply their control inputs u_A and u_B as defined in equation (4.12) with i replaced by A and B, respectively, based on given velocities $v_A^{new} \in ORCA_{AB}^{\tau}$ and $v_B^{new} \in ORCA_{BA}^{\tau}$, where $ORCA_{AB}^{\tau}$ is computed as*

$$ORCA_{AB}^{\tau} = \left\{ v \,\middle|\, \left(v - \left(v_A^{pref} + \frac{1}{2} w \right) \right) \cdot n > 0 \right\}, \tag{4.40}$$

and $ORCA_{BA}^{\tau}$ is computed as

$$ORCA_{BA}^{\tau} = \left\{ v \,\middle|\, \left(v - \left(v_B^{pref} - \frac{1}{2} w \right) \right) \cdot (-n) > 0 \right\}, \tag{4.41}$$

with w as defined in equation (4.37) and where n is the outward normal vector of $\partial \mathcal{VO}_{AB}^{\tau}$ at

$$p = \underset{v \in \partial \mathcal{VO}_{AB}^{\tau}}{argmin} \left\| v - v_{AB}^{pref} \right\|. \tag{4.42}$$

Assume that v_A^{new} and v_B^{new} are constant for a time horizon τ and that the constraint (4.8) is satisfied for both $\xi_{d(A)}$ and $\xi_{d(B)}$. Then A and B do not collide before τ, i.e.,

$$v_A - v_B \notin \mathcal{VO}_{AB}^{\tau}. \tag{4.43}$$

Proof. Using equation (4.20) with v_A^{pref} replaced by v_A^{new} and v_B^{pref} replaced by v_B^{new},

$$v_A = v_A^{new} - \xi_{d(A)} \tag{4.44}$$

and

$$v_B = v_B^{new} - \xi_{d(B)}. \tag{4.45}$$

Choosing new velocities $v_A^{new} \in ORCA_{AB}^{\tau}$ (equation (4.40)) and $v_B^{new} \in ORCA_{BA}^{\tau}$ (equation (4.41)) must satisfy

$$\left(v_A^{new} - \left(v_A^{pref} + \frac{1}{2} w \right) \right) \cdot n > 0 \tag{4.46}$$

and

$$\left(v_B^{new} - \left(v_B^{pref} - \frac{1}{2}w\right)\right) \cdot (-n) > 0. \tag{4.47}$$

Solving (4.44) and (4.45) for v_A^{new} and v_B^{new}, respectively, and inserting them in (4.46) and (4.47) yields

$$\left(v_A + \xi_{d(A)} - \left(v_A^{pref} + \frac{1}{2}w\right)\right) \cdot n > 0 \tag{4.48}$$

and

$$\left(v_B + \xi_{d(B)} - \left(v_B^{pref} - \frac{1}{2}w\right)\right) \cdot (-n) > 0. \tag{4.49}$$

Adding (4.48) and (4.49) gives

$$\left(v_A - v_B + \xi_{d(A)} - \xi_{d(B)} - v_A^{pref} + v_B^{pref} - w\right) \cdot n > 0. \tag{4.50}$$

Using (4.16) then yields

$$\left(v_A - v_B + \xi_{d(A)} - \xi_{d(B)} - v_{AB}^{pref} - w\right) \cdot n > 0, \tag{4.51}$$

Define

$$e = w - d, \tag{4.52}$$

where w is defined in (4.38) and d is defined in (4.33). Using equations (4.33) and (4.52), (4.51) can be rewritten as

$$\big(v_A - v_B + \xi_{d(A)} - \xi_{d(B)} - (p + e)\big) \cdot n > 0. \tag{4.53}$$

Rearranging yields

$$(v_A - v_B - p) \cdot n > \big(e - \xi_{d(A)} + \xi_{d(B)}\big) \cdot n. \tag{4.54}$$

From (4.34), (4.38), and (4.52)

$$e = kn,\ \ k > 0. \tag{4.55}$$

Therefore, since $\mathcal{VO}^{\tau}_{AB}$ is a closed set while π is an open set,

$$e \cdot n = \|e\| > 0. \tag{4.56}$$

Due to symmetry of ε_A and ε_B,

$$\varepsilon^{diff}_{AB} = \varepsilon_A - \varepsilon_B = \varepsilon_A + (-\varepsilon_B) = \varepsilon_A + \varepsilon_B = \varepsilon^{sum}_{AB}, \tag{4.57}$$

where ε^{sum}_{AB} is defined in (4.17).

Define an orthogonal coordinate system with origin at $v^{pref}_{AB} + w$ and with its primary axis along n, and consider the coordinate of $\xi_{d(A)} - \xi_{d(B)}$ along this axis, i.e., $(\xi_{d(A)} - \xi_{d(B)}) \cdot n$. Then there are two cases,

1. $(\xi_{d(A)} - \xi_{d(B)}) \cdot n \leq 0$,
2. $(\xi_{d(A)} - \xi_{d(B)}) \cdot n > 0$.

Using (4.56), for case 1 we can conclude that

$$\|e\| = e \cdot n > (\xi_{d(A)} - \xi_{d(B)}) \cdot n. \tag{4.58}$$

We will now prove by contradiction that this result still stands for case 2. To that aim, we first notice that, due to the symmetry of ε^{sum}_{AB}, for any $\xi_{d(A)} - \xi_{d(B)}$ in case 2 there is a corresponding point $\xi_{d(B)} - \xi_{d(A)}$ with negative coordinate along n, i.e.,

$$(\xi_{d(B)} - \xi_{d(A)}) \cdot n = -(\xi_{d(A)} - \xi_{d(B)}) \cdot n < 0. \tag{4.59}$$

Assume that there are $\xi^*_{d(A)}$ and $\xi^*_{d(B)}$ in case 2 such that $(\xi^*_{d(A)} - \xi^*_{d(B)}) \cdot n \geq \|e\|$. Then, this would imply that $\xi^*_{d(B)} - \xi^*_{d(A)} \in \mathcal{VO}^{\tau}_{AB}$ and therefore $\xi^*_{d(B)} - \xi^*_{d(B)} \notin \pi$, which violates the constraint in (4.37). Note that the constraint in (4.37) is on $\overline{\varepsilon^{sum}_{AB}} + w$, which is a shifted version of ε_{AB}^{sum}. From case 1 and case 2 we can conclude that

$$e \cdot n > \left(\xi_{d(A)} - \xi_{d(B)}\right) \cdot n. \tag{4.60}$$

Rearranging equation (4.60) yields

$$\left(e - \xi_{d(A)} + \xi_{d(B)}\right) \cdot n > 0. \tag{4.61}$$

Using equations (4.54) and (4.61) leads to

$$(v_A - v_B - p) \cdot n > 0, \tag{4.62}$$

From (4.62) and (4.35),

$$v_A - v_B \in \pi. \tag{4.63}$$

Then, using equation (4.36) we conclude that (4.43) is satisfied. □

Corollary 4.2. *Consider m agents $A, B_1, ..., B_{m-1}$ operating within the same area. Let A choose its new velocity $v_A^{new} \in ORCA_A^\tau$, where*

$$v_A = v_A^{new} - \xi_{d(A)} \tag{4.64}$$

and $ORCA_A^\tau$ is defined in equation (2.28) and repeated here for convenience,

$$ORCA_A^\tau = D(0, v_A^{max}) \cap \bigcap_{i=1}^{m-1} ORCA_{AB_i}^\tau, \tag{4.65}$$

with $ORCA_{AB_i}^\tau$ computed using w as defined in equation (4.37) and where n is the outward normal vector of $\partial \mathcal{VO}_{AB}^\tau$ at

$$p = \underset{v \in \partial \mathcal{VO}_{AB}^\tau}{argmin} \left\| v - v_{AB}^{pref} \right\|. \tag{4.66}$$

Then assuming that v_A^{new} and $v_{B_i}^{new}$ are constant for a time horizon τ and that the constraint

(4.8) is satisfied for both $\xi_{d(A)}$ and $\xi_{d(B_i)}$, A will not collide with any other agent $B_i, i \in \{1, ..., m-1\}$ that chooses a new velocity $v_{B_i}^{new} \in ORCA_{B_iA}^{\tau}$, i.e.,

$$v_A - v_{B_i} \notin \mathcal{VO}_{AB_i}^{\tau}, \forall i \in \{1, ..., m-1\}, \tag{4.67}$$

where

$$v_{B_i} = v_{B_i}^{new} - \xi_{d(B_i)}. \tag{4.68}$$

Proof. From the definition of $ORCA_A^{\tau}$ (equation (4.65)), assuming that v_A^{max} is finite,

$$ORCA_A^{\tau} \subset ORCA_{AB_i}^{\tau}, \forall i \in \{1, ..., m-1\}. \tag{4.69}$$

Therefore, $v_A^{new} \in ORCA_A^{\tau}$ implies that $v_A^{new} \in ORCA_{AB_i}^{\tau}$. From Theorem 4.3, we know that $v_A^{new} \in ORCA_{AB_i}^{\tau}$ and $v_{B_i}^{new} \in ORCA_{B_iA}^{\tau}$ leads to (4.67). □

4.4 Algorithm for Collision-free Multi-Swarm Coverage Control with Uncertainty

The proposed algorithm to use the method proposed in 4.3 for collision-free multi-swarm coverage control with bounded disturbance measurement uncertainties is shown in table 2. The set D contains the disturbance measurements. We adopt the same notation and make the same assumptions as in section 3.5:

1. Planar motion of the agents is assumed. For flying vehicles such as UAVs, this corresponds to the scenario where all agents operate at the same constant altitude.

2. All swarms use the same algorithm to cover the area and avoid other vehicles.

3. The computations are executed synchronously for all agents.

4. Group affiliation, as well as the radius of the circle that defines a safety zone, is known for each agent.

5. Knowledge regarding the locations of all other agents within the same swarm can be obtained through communication between vehicles.

6. Knowledge regarding the locations of all agents from other swarms can be obtained using sensors.

7. The input needed to counteract disturbances can always be achieved.

Algorithm 2 Computation of a Collision-Free Control Input for an Agent in a Multi-Swarm Coverage Control Scenario

```
**Input:** $X, Q, D$
**Output:** $u_{i,j}^{new}$
$X, D \leftarrow$ update($X, D$);
$x_{i,j} \leftarrow X_j(i)$;
$Edges_j, Vertices_j \leftarrow$ voronoi($X_j, Q$);
$CM_{V_{i,j}} \leftarrow$ centerOfMass($Edges_j(i), Vertices_j(i)$);
$v_{i,j}^{pref} \leftarrow$ desiredVelocity($CM_{V_{i,j}}, x_{i,j}, k_{i,j}$);
$\hat{v}_{d(i,j)} \leftarrow$ estimateDisturbances(D);
**for all** $X_l \subset X$, $l = \{1, ..., N\}$ **do**
    $Edges_l, Vertices_l \leftarrow$ voronoi($X_l, Q$);
    **for all** $x_{k,l} \in X_l, \forall\,(k,l) \neq (i,j), k = \{1, ..., m\}$ **do**
        $CM_{V_{k,l}} \leftarrow$ centerOfMass($Edges_l(k), Vertices_l(k)$);
        $\hat{v}_{k,l}^{pref} \leftarrow$ desiredVelocity($CM_{V_{k,l}}, x_{k,l}, \hat{k}_{k,l}$);
        $\mathcal{VO}_{(i,j)(k,l)}^{\tau} \leftarrow$ velocityObstacle($x_{i,j}, x_{k,l}, r_{i,j}, r_{k,l}, \tau$);
        $v_{(i,j)(k,l)}^{pref} \leftarrow v_{i,j}^{pref} - \hat{v}_{k,l}^{pref}$;
        $\varepsilon_{i,j}, \varepsilon_{k,l} \leftarrow$ uncertaintyEllipses($\xi_{d(i,j)}, \xi_{d(k,l)}$);
        $\overline{\varepsilon_{(i,j)(k,l)}^{sum}} \leftarrow \varepsilon_{i,j} + \varepsilon_{k,l} + v_{(i,j)(k,l)}^{pref}$;
        $ORCA_{(i,j)(k,l)}^{\tau} \leftarrow$ halfplane($\mathcal{VO}_{(i,j)(k,l)}^{\tau}, \overline{\varepsilon_{(i,j)(k,l)}^{sum}}, v_{(i,j)(k,l)}^{pref}$);
        $ORCA_{(i,j)(l)}^{\tau} \leftarrow \bigcap_{k=1}^{m} ORCA_{(i,j)(k,l)}^{\tau}$;
    **end for**
    $ORCA_{i,j}^{\tau} \leftarrow D(0, v_{i,j}^{max}) \cap \bigcap_{l=1}^{N-1} ORCA_{(i,j)(l)}^{\tau}$;
**end for**
$v_{i,j}^{new} \leftarrow$ newVelocity($ORCA_{i,j}^{\tau}$);
$u_{i,j}^{new} \leftarrow v_{i,j}^{new} - \hat{v}_{d(i,j)}$;
**return** $u_{i,j}^{new}$
```

As mentioned previously, assumption 6 can be achieved, for example, by using multiple agents within the same swarm to sense their distance to an agent that belongs to another swarm and doing respective computations.

In lines 1 and 2 of the algorithm, the positions of the agents and the disturbance measurements across the area are updated. The Voronoi tessellation, as well as the centers of mass of the Voronoi cells, are computed in lines 3 and 4. Subsequently, the agent i, j that executes the algorithm determines its desired velocity using the coverage control strategy (equation (2.9) or (2.13)) and estimates the velocity of the disturbance at its location using equation (4.4) (lines 5,6). In lines 7-21, the agent calculates its set of feasible velocities considering all other agents. More specifically, for each swarm, after computing the edges and vertices of the respective Voronoi cells in line 9, the centers of mass of the Voronoi cells (equation (2.6)) are computed in line 10. Furthermore, the desired velocity of each agent is estimated using coverage control methods such as equations (2.9) and (2.13) (line 11). Subsequently, the velocity obstacle of agent i, j with respect to each other agent is obtained following equation (4.15) (line 12). The relative velocity between i, j and each other agent is then determined (line 13), before their uncertainty ellipses are computed (equation (4.9)) along with the translated Minkowski sum as defined in equation (4.18) in lines 14 and 15. Consequently, the half-plane $ORCA^{\tau}_{(i,j)(k,l)}$ is calculated (equation (4.40)), and the set of feasible velocities is obtained by intersecting the half-planes with respect to all agents (lines 16-20). Finally (lines 22, 23)), agent i, j computes its new velocity (equation (2.29)), along with a new control input.

4.5 Simulations

This section presents simulations to validate the proposed methodology and algorithm introduced in sections 4.3 and 4.4, respectively. As in chapter 3, the simulations were performed in MATLAB R2019a on a laptop possessing 16 GB of RAM as well as an Intel Core i7-1255U

CPU with base speed 1.7 GHz.

For all simulations, the same area Q as in Examples 3.1 and 3.3 is considered, whose boundary has its vertices at $[(1,0),(6,0),(8,5),(5,8),(0,4)]$. Simulations were executed for two non-cooperating swarms aiming to provide coverage to a common area. Each swarm consists of four agents that start at different sets of initial conditions. Again, notice that all algorithms proposed in this thesis are general for any number of swarms. For simplicity, only simulations with two swarms are presented. Moreover, the swarms do not need to contain the same number of agents.

In contrast to Example 3.3, the area is subject to a field of disturbance. For the simulations, we assume that measurements of the disturbance at each point within Q as well as an estimate of the bias are available. Uncertainty is described by a bounded ellipse. The agents compute their desired velocities using equation (2.13) with $s_{i,j} = r_{i,j} = 1, \forall i \in \{1,...,m\}, \forall j \in \{1,...,N\}$. The time horizon τ chosen for collision avoidance is one time step. The results obtained for one specific combination of the wind field and the initial positions of the agents is presented in Example 4.1.

Example 4.1. *In this example, two independent swarms, each consisting of four agents, execute the coverage task within a common area where disturbance is present. Collision avoidance is implemented using the methodology and algorithm presented in sections 4.3 and 4.4, respectively. Consider the same area with uniform density distribution and the same conditions as in Examples 3.1 and 3.3. The agents are placed at the following initial positions:*

- *Swarm 1 (S1):* $[(2,1),(2,1.5),(2.5,1),(2.5,1.5)]$,
- *Swarm 2 (S2):* $[(5,6),(5,6.5),(5.5,6),(5.5,6.5)]$.

The radii of the safety zones of all agents are 0.2 units. Similarly to Example 3.3, the time step between computations is chosen to be 0.01 units of time, and the time horizon τ is one time step. As before, the desired velocity for each agent is computed using equation (2.13) with $s_{i,j} = r_{i,j} = 1, \forall i \in \{1,...,m\}, \forall j \in \{1,...,N\}$.

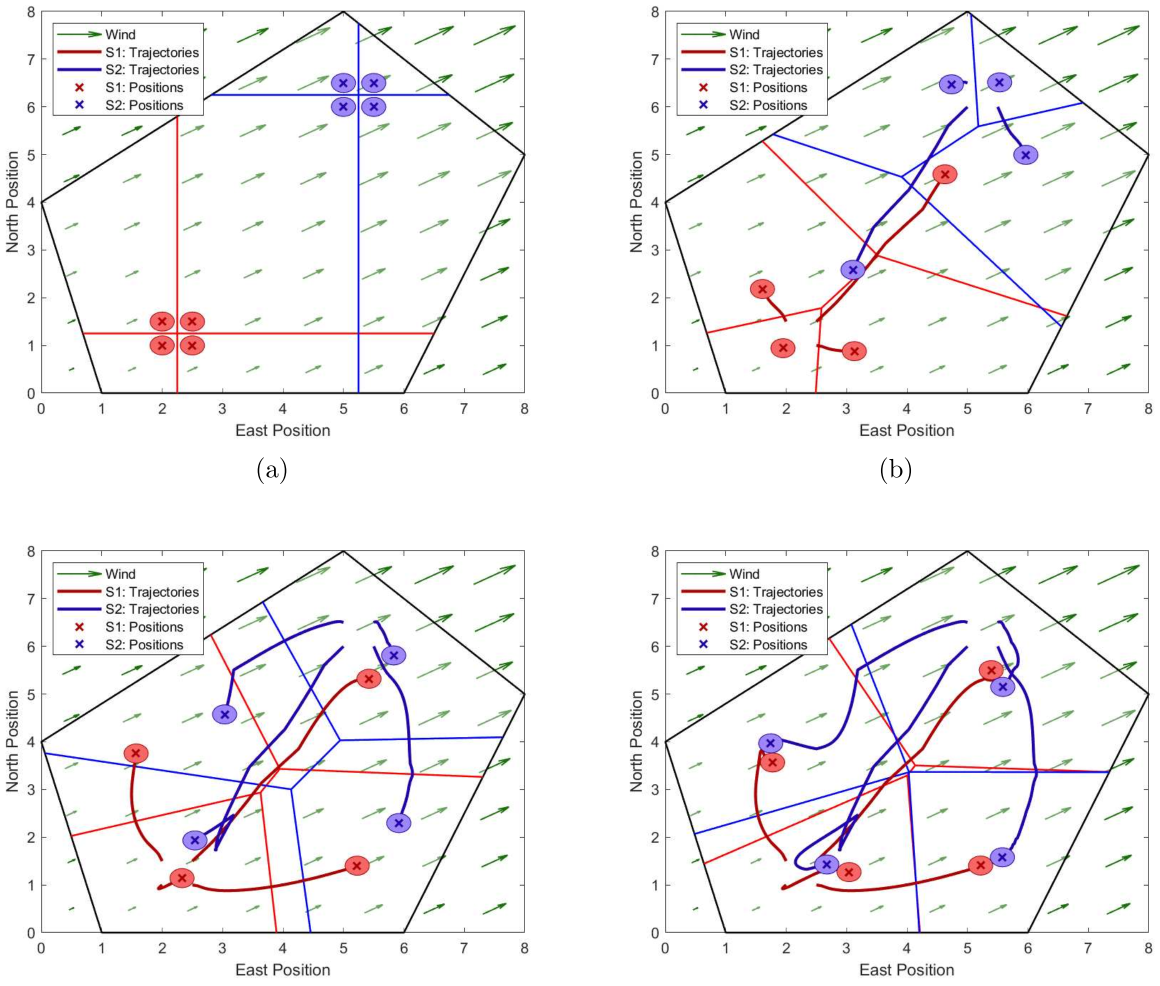

(a)

(b)

(c)

(d)

Figure 4.3: Simulation of coverage control with two non-cooperating swarms moving in a non-uniform wind field showing the trajectories and positions of the agents of swarm 1 (S1) and swarm 2 (S2) (a) at the first time step (b) after 10 time steps (c) after 50 time steps (d) after convergence to their final positions.

Different from the previous examples, a non-uniform velocity disturbance field is present. While the direction of all disturbances is 30 degrees, as measured from the east axis, the magnitude of the disturbance speed $v_{d(i)}(x, y)$ increases linearly towards the east and north, and for this simulation, it is defined by the following function: $v_{d(i)}(x, y) = 0.05(x + y) + 0.1$, *where x represents the east position and y represents the north position. Regarding the* *measurements of the disturbances, the estimate of the bias depends on the disturbance speed,*

$$\hat{b}_{d(i)} = 0.01 v_{d(i)}. \tag{4.70}$$

Similarly, the semi-major axis a_1 *of the uncertainty ellipse depends on the speed of disturbance,*

$$a_1 = \left(0.05 \left\| v_{d(i)} \right\|\right)/2, \tag{4.71}$$

and aligns with the direction of the disturbance. The perpendicular semi-minor axis a_2 *is*

$$a_2 = \left(0.02 \left\| v_{d(i)} \right\|\right)/2. \tag{4.72}$$

The positions and trajectories of the agents can be seen in figure 4.3. The agents are depicted at their initial positions in figure 4.3a. Figures 4.3b and 4.3c show the agents' positions and trajectories after 10 and 50 time steps, respectively. Moreover, the agents are displayed after convergence to their final positions in figure 4.3d, along with the trajectories traveled. It can be seen that the agents do not collide with each other and that they converge to similar positions as in Example 3.3. Another interesting observation is that the trajectories traveled by the agents are similar to those traveled in Example 3.3. This supports that using the proposed collision avoidance methodology and algorithm does not significantly influence the trajectories unless necessary for collision avoidance.

In summary, the results show that the proposed method guarantees collision-free motion in multi-swarm coverage control scenarios. This does not only apply to environments without disturbances, but also to the case where disturbances are present and measurements of those disturbances are subject to noise. No major differences between the trajectories taken by agents in both scenarios are visible, which suggests that, compared to the example without disturbance, the proposed methodology does not have a negative impact on the quality of coverage achieved by each swarm.

Chapter 5

Conclusions and Future Work

5.1 Summary

This thesis analyzed the problem of coverage control with multiple non-cooperating swarms. The work shows that multi-swarm coverage control is a promising solution for applications including wildfire mitigation, planetary exploration, and mobile coverage, where swarms of multiple agents operate within a shared area. Playing an important role for safe operation in such scenarios, collision avoidance can be achieved, for example, through methods based on ORCA [4]. Despite pairs of agents from different swarms moving to similar desired locations, the methodologies proposed in this thesis guarantee collision-free motion for agents involved in the coverage task. This applies to both disturbance-free environments as well as areas where disturbances such as wind are present, and when their measurements include noise. Depending on the control architecture, computational performance may become a challenge in multi-swarm coverage control as the number of agents operating within the same area increases. In contrast, a possibility to increase the energy efficiency of the agents involved in the task that has not been addressed in this thesis is the use of disturbances to reduce the energy consumption. These and other considerations lead to the following ideas for extensions that build on the results presented in this thesis:

- Extension to three-dimensional scenarios,
- Development of strategies to increase computational efficiency,
- Incorporation of non-uniform density distributions over the area to be covered,
- Extension to account for uncertainty in both positions and velocities of the agents at the same time,
- Taking advantage of external disturbances such as wind to increase the energy efficiency of the agents,
- Application of the proposed collision avoidance methodology with bounded disturbance uncertainty to scenarios independent of coverage control.

Bibliography

[1] "Canadian Wildland Fire Information System | Canadian National Fire Database (CNFDB) — cwfis.cfs.nrcan.gc.ca," https://cwfis.cfs.nrcan.gc.ca/ha/nfdb?type=poly\&year=2023, [Accessed 17-04-2025].

[2] M. Bartels, "NASA's Mars Helicopter Ingenuity Ends Mission on the Red Planet after 3 Years — scientificamerican.com," https://www.scientificamerican.com/article/nasa-rsquo-s-mars-helicopter-ingenuity-ends-mission-on-the-red-planet-after-3-years/, [Accessed 17-04-2025].

[3] P. Fiorini, "Motion planning in dynamic environments using velocity obstacles," *The International Journal of Robotics Research*, vol. 17, pp. 760–772, 07 1998.

[4] J. van den Berg, S. J. Guy, M. Lin, and D. Manocha, "Reciprocal n-body collision avoidance," in *Robotics Research*, C. Pradalier, R. Siegwart, and G. Hirzinger, Eds. Berlin, Heidelberg: Springer Berlin Heidelberg, 2011, pp. 3–19.

[5] "Canada - Record wildfires spread to urban areas — internal-displacement.org," https://www.internal-displacement.org/spotlights/canada-record-wildfires-spread-to-urban-areas/, [Accessed 27-03-2025].

[6] "Canada's record-breaking wildfires in 2023: A fiery wake-up call," https://natural-resources.canada.ca/stories/simply-science/canada-s-record-breaking-wildfires-2023-fiery-wake-call, [Accessed 27-03-2025].

[7] "How much forest does Canada have? - Natural Resources Canada — natural-resources.canada.ca," https://natural-resources.canada.ca/forest-forestry/much-forest-does-canada-have, [Accessed 27-03-2025].

[8] "Wildfires — who.int," https://www.who.int/health-topics/wildfires#tab=tab_2, [Accessed 27-03-2025].

[9] E. Ausonio, P. Bagnerini, and M. Ghio, "Drone swarms in fire suppression activities: A conceptual framework," *Drones*, vol. 5, no. 1, 2021. [Online]. Available: https://www.mdpi.com/2504-446X/5/1/17

[10] "The History of the Space Race — education.nationalgeographic.org," https://education.nationalgeographic.org/resource/history-space-exploration/, [Accessed 28-03-2025].

[11] "NASA - NSSDCA - Spacecraft - Details — nssdc.gsfc.nasa.gov," https://nssdc.gsfc.nasa.gov/nmc/spacecraft/display.action?id=2020-052A, [Accessed 29-03-2025].

[12] "Every mission to Mars ever — planetary.org," https://www.planetary.org/space-missions/every-mars-mission, [Accessed 29-03-2025].

[13] "Tianwen-3: China's Mars sample return mission — planetary.org," https://www.planetary.org/articles/tianwen-3-china-mars-sample-return-mission, [Accessed 30-03-2025].

[14] "ExoMars — esa.int," https://www.esa.int/Science_Exploration/Human_and_Robotic_Exploration/Exploration/ExoMars, [Accessed 30-03-2025].

[15] "Marsbee — marsbee.uah.edu," https://marsbee.uah.edu/, [Accessed 30-03-2025].

[16] A. Petrovsky, I. Kalinov, P. Karpyshev, D. Tsetserukou, A. Ivanov, and A. Golkar, "The two-wheeled robotic swarm concept for mars exploration," *Acta Astronautica*,

vol. 194, pp. 1–8, 2022. [Online]. Available: https://www.sciencedirect.com/science/article/pii/S0094576522000340

[17] M. O.-E. Aoueileyine, R. Allani, R. Bouallegue, and A. Yazidi, "Coverage strategy for small-cell uav-based networks in iot environment," *Sensors*, vol. 23, no. 21, 2023. [Online]. Available: https://www.mdpi.com/1424-8220/23/21/8771

[18] "Airborne Base Stations Bring Back Connectivity - ZTE — gsma.com," https://www.gsma.com/get-involved/gsma-foundry/gsma_resources/airborne-base-stations-bring-back-connectivity-zte/, [Accessed 02-04-2025].

[19] D. T. AG, "Deutsche Telekom uses drone as flying base station for temporary coverage — telekom.com," https://www.telekom.com/en/media/media-information/archive/deutsche-telekom-uses-drone-as-flying-base-station-for-temporary-coverage-1088440, [Accessed 01-04-2025].

[20] J. Cortés, S. Martinez, T. Karatas, and F. Bullo, "Coverage control for mobile sensing networks," *IEEE Transactions on Robotics and Automation*, vol. 20, no. 2, pp. 243–255, 2004.

[21] J. Cortés, S. Martínez, and F. Bullo, "Spatially-distributed coverage optimization and control with limited-range interactions," *http://dx.doi.org/10.1051/cocv:2005024*, vol. 11, 01 2004.

[22] S. Lloyd, "Least squares quantization in pcm," *IEEE Transactions on Information Theory*, vol. 28, no. 2, pp. 129–137, 1982.

[23] Q. Du, V. Faber, and M. Gunzburger, "Centroidal voronoi tessellations: Applications and algorithms," *SIAM Review*, vol. 41, no. 4, pp. 637–676, 1999. [Online]. Available: https://doi.org/10.1137/S0036144599352836

[24] M. Moarref and L. Rodrigues, "An optimal control approach to decentralized energy-efficient coverage problems," *IFAC Proceedings Volumes*, vol. 47, no. 3,

pp. 6038–6043, 2014, 19th IFAC World Congress. [Online]. Available: https://www.sciencedirect.com/science/article/pii/S1474667016425577

[25] M. T. Nguyen, L. Rodrigues, C. S. Maniu, and S. Olaru, "Discretized optimal control approach for dynamic multi-agent decentralized coverage," in *2016 IEEE International Symposium on Intelligent Control (ISIC)*, 2016, pp. 1–6.

[26] M. Di Perna and L. Rodrigues, "Distributed backstepping coverage control for multi-agents moving on a plane," in *2017 IEEE 56th Annual Conference on Decision and Control (CDC)*, 2017, pp. 1590–1595.

[27] S. F. Chaitra, B. Yang, and S. Mikhail, "Safe coverage control for multi-agent systems," in *2023 62nd Annual Conference of the Society of Instrument and Control Engineers (SICE)*, 2023, pp. 1394–1399.

[28] Y. Yang, Y. Liang, and Y. Zhao, "An analytical solution for obstacle avoidance in cooperative area coverage using UAV swarms," in *2024 36th Chinese Control and Decision Conference (CCDC)*, 2024, pp. 2432–2437.

[29] R. Haghighi and C. Cheah, "Multi-group coordination control for robot swarms," *Automatica*, vol. 48, no. 10, pp. 2526–2534, 2012. [Online]. Available: https://www.sciencedirect.com/science/article/pii/S0005109812002658

[30] F. Sharifi, "Cooperative coverage control of multi-agent systems," Ph.D. dissertation, Concordia University, September 2014, unpublished. [Online]. Available: https://spectrum.library.concordia.ca/id/eprint/979009/

[31] G. M. Atınç, D. M. Stipanović, and P. G. Voulgaris, "A swarm-based approach to dynamic coverage control of multi-agent systems," *Automatica*, vol. 112, p. 108637, 2020. [Online]. Available: https://www.sciencedirect.com/science/article/pii/S0005109819304984

[32] Q. Wang and H. Zhang, "A self-organizing area coverage method for swarm robots based on gradient and grouping," *Symmetry*, vol. 13, no. 4, 2021. [Online]. Available: https://www.mdpi.com/2073-8994/13/4/680

[33] C. Song and Y. Fan, "Coverage control for mobile sensor networks subject to bounded measurement errors," in *2020 39th Chinese Control Conference (CCC)*, 2020, pp. 4864–4869.

[34] J. Chen and P. Dames, "Distributed and collision-free coverage control of a team of mobile sensors using the convex uncertain voronoi diagram," in *2020 American Control Conference (ACC)*, 2020, pp. 5307–5313.

[35] Y. Bai, Y. Wang, M. Svinin, E. Magid, and R. Sun, "Adaptive multi-agent coverage control with obstacle avoidance," *IEEE Control Systems Letters*, vol. 6, pp. 944–949, 2022.

[36] Y. Bai, Y. Wang, X. Xiong, J. Song, and M. Svinin, "Safe adaptive multi-agent coverage control," *IEEE Control Systems Letters*, vol. 7, pp. 3217–3222, 2023.

[37] J. van den Berg, M. Lin, and D. Manocha, "Reciprocal velocity obstacles for real-time multi-agent navigation," in *2008 IEEE International Conference on Robotics and Automation*, 2008, pp. 1928–1935.

[38] S. J. Guy, J. Chhugani, C. Kim, N. Satish, M. Lin, D. Manocha, and P. Dubey, "Clearpath: highly parallel collision avoidance for multi-agent simulation," in *Proceedings of the 2009 ACM SIGGRAPH/Eurographics Symposium on Computer Animation*, ser. SCA '09. New York, NY, USA: Association for Computing Machinery, 2009, p. 177–187. [Online]. Available: https://doi.org/10.1145/1599470.1599494

[39] F. Vesentini, R. Muradore, and P. Fiorini, "A survey on velocity obstacle paradigm," *Robotics and Autonomous Systems*, vol. 174, p. 104645, 02 2024.

[40] J. Ellingson, E. Pitts, C. K. Peterson, K. Warnick, and T. McLain, “Uncertainty velocity obstacle avoidance for sUAS trajectory planning in a 2d plane,” in *2020 IEEE Aerospace Conference*, 2020, pp. 1–11.

[41] Z. Gyenes and E. G. Szádeczky-Kardoss, “Motion planning for mobile robots using uncertain estimations about the environment,” in *2020 23rd International Symposium on Measurement and Control in Robotics (ISMCR)*, 2020, pp. 1–6.

[42] X. Zhang, J. Ma, Z. Cheng, M. Tomizuka, and T. H. Lee, “Velocity obstacle based risk-bounded motion planning for stochastic multi-agent systems,” 2022.

[43] E. J. Rodríguez-Seda, D. M. Stipanović, and M. W. Spong, “Collision avoidance control with sensing uncertainties,” in *Proceedings of the 2011 American Control Conference*, 2011, pp. 3363–3368.

[44] S. Boddu, S. Suman, and S. De, “Impact of wind on UAV collision avoidance,” in *ICC 2024 - IEEE International Conference on Communications*, 2024, pp. 2592–2597.

[45] A. Pierson and D. Rus, “Distributed target tracking in cluttered environments with guaranteed collision avoidance,” in *2017 International Symposium on Multi-Robot and Multi-Agent Systems (MRS)*, 2017, pp. 83–89.

[46] S. Boyd and L. Vandenberghe, *Convex optimization.* Cambridge university press, 2004.